THE UNIVERSITY OF MICHIGAN

COLLEGE OF ENGINEERING
Department of Aeronautical and Astronautical Engineering
Aerodynamics Laboratory

Technical Report

MEASUREMENTS OF THE CORRELATION BETWEEN THE FLUCTUATING VELOCITIES AND THE FLUCTUATING WALL PRESSURE IN A THICK TURBULENT BOUNDARY LAYER

C. E. Wooldridge
W. W. Willmarth

ORA Project 02920

under contract with:

DEPARTMENT OF THE NAVY
OFFICE OF NAVAL RESEARCH
CONTRACT NO. Nonr-1224(30)
WASHINGTON, D. C.

administered through:

OFFICE OF RESEARCH ADMINISTRATION ANN ARBOR

April 1962

This report was also a dissertation submitted in partial fulfillment of the requirements for the degree of Doctor of Philosophy in The University of Michigan, 1962.

TABLE OF CONTENTS

TABLE OF CONTENTS (Concluded)

LIST OF ILLUSTRATIONS

LIST OF ILLUSTRATIONS (Continued)

NOMENCLATURE

$E_p(\omega)$	power spectrum of the wall pressure
$E_u(\omega)$	power spectrum of longitudinal velocity fluctuation
$E_v(\omega)$	power spectrum of velocity fluctuation normal to plate
f	frequency
k	wave number; $k = \frac{\omega}{U}$
$\mathscr{P}$	total pressure, mean plus fluctuating; see Eq. (7)
p	fluctuating wall pressure
R	Reynolds number based on distance from virtual origin of turbulent boundary layer
R_θ	Reynolds number based on momentum thickness
R_{pu}, R_{pv}, R_{pw}	normalized wall pressure-velocity correlations; see, e.g., Eqs. (4) and (5)
$R_{p\dot{v}}$	normalized correlation of wall pressure with time derivative of velocity normal to wall; see Eq. (11)
R_{pv_x}	normalized correlation of wall pressure with longitudinal spatial derivative of velocity normal to wall, see Eq. (9)
$R'_{pu}, R'_{pv}, R'_{pw}$	standardized correlations normalized on the velocity field at $y/\delta^* = 0.51$
R_{pp}	normalized wall pressure correlation
R_{uu}, R_{vv}	normalized velocity-velocity correlations
U	mean velocity in the boundary layer in the stream direction
U_∞	free-stream velocity
U_τ	wall friction velocity
U_c	convection speed of the fluctuating velocity field which is correlated with fluctuating wall pressure

NOMENCLATURE (Continued)

$\mathcal{U}$	total velocity, mean plus fluctuating; see Eq. (7)
u,v,w	fluctuating velocities x,y,z directions
$\dot{v}$	time derivative of velocity fluctuation normal to wall
v_x	longitudinal spatial derivative of velocity fluctuation normal to wall
x_1,x_2,x_3	spatial separations of pressure and velocity transducers in x,y,z directions
x	distance parallel to wall, increasing in the stream direction
y	distance normal to wall, increasing away from wall
z	distance parallel to wall and perpendicular to stream, forming a right-hand Cartesian coordinate system with x and y
δ	boundary layer thickness
δ^*	boundary layer displacement thickness
θ	boundary layer momentum thickness
$(\Lambda_{pu})_i,(\Lambda_{pv})_i$	integral scales of R_{pu} and R_{pv} in x_i-direction; i = 1,2,3
$(\Lambda_{p\dot{v}})_i$	integral scale of $R_{p\dot{v}}$ in x_i-direction; i = 1,2,3
$(\Lambda_{uu})_i$	integral scale of R_{uu} in x_i-direction; i = 1,2,3
$(\Lambda_{pp})_i$	integral scale of R_{pp} in x_i-direction; i = 1,3
ν	kinematic viscosity
ρ	density
τ	time delay
τ'	time delay equal to transducer spacing divided by local speed

NOMENCLATURE (Concluded)

ω	circular frequency; $\omega = 2\pi f$
$\overline{(\ )}$	time average

ABSTRACT

The purpose of this investigation was to gain additional knowledge about the structure of the turbulent boundary layer flow. Turbulent motion in a thick (5 inch) boundary layer with zero longitudinal pressure gradient which is produced by natural transition on a smooth surface has been studied. Measurements have been made of the space-time correlations between the fluctuating wall pressure and the fluctuating velocities in the layer, and between the fluctuating wall pressure and the time derivative of the fluctuating velocity normal to the wall.

A study of the data of other investigators as compared to the data obtained in the present experiments shows that some features of the turbulent structure obtained in many of the previous investigations in tripped boundary layers were not always universal but were a function of the experimental conditions imposed by the tripping device.

At any height in the boundary layer the convection speed of the velocity disturbance which was correlated with the wall pressure disturbances was the local mean speed. The correlation of the wall pressure with the longitudinal velocity was opposite in sign to the correlation of the pressure with the velocity normal to the wall. This implies that the part of the velocity field which is correlated with the wall pressure also acts to produce turbulent shear.

The integral scales of the pressure-velocity correlation extend approximately one boundary layer thickness along the stream and 0.2 of a boundary layer thickness in the other two perpendicular directions.

The wall pressure is an integral of the longitudinal spatial derivative of the velocity normal to the wall over all space. This spatial derivative can be related to the time derivative through the convection speed. The measurement of the pressure-velocity time-derivative correlation shows that most of the wall pressure is produced by velocity fluctuations near the surface. The correlation has a measurable value only in the inner 0.4 of the boundary layer. This is in agreement with the fact that the final value of the wall pressure convection speed which is reached at large spacing between the points of measurement, as measured by many investigators, is only about 0.8 of the free-stream speed. This speed occurs at approximately 0.2 of the boundary layer thickness.

The integral scales of the pressure-velocity derivative correlation are smaller than those of the pressure-velocity correlations. These scales are approximately 0.2 of the boundary layer thickness along the stream and 0.15 of the boundary layer thickness in the other two perpendicular directions.

A vector field of the pressure-velocity correlation data is presented. The hypothesis is made that this field represents the velocity field generated by a superposition of eddies of all sizes whose axes lie parallel to the wall and perpendicular to the mean velocity which are in contact with a layer of fluid near the wall.

I. INTRODUCTION

The structure of wall turbulence is not yet well understood from either a theoretical or an experimental point of view. Further development of the theory will depend upon use of the knowledge gained from experimental measurements. Previous experimental investigations of the structure of the turbulence, some of which are summarized below, have been concerned with measurements of either the fluctuating velocity field or the fluctuating wall pressure field. The present investigation is concerned with the relation between the velocity field and the wall pressure.

One of the first extensive investigations of velocity fluctuations in a turbulent boundary layer was made by Townsend.[1] He found that the principal energy-containing eddies were attached to the wall and lost their energy through direct viscous dissipation near the wall.

Later Grant[2] measured the spatial correlations of the three fluctuating turbulent velocities with themselves. Evidence was found of jet-like stress relieving motions originating over a large range of distances from the wall and squirting outward and downstream away from the wall.

Favre, Gaviglio, and Dumas[3,4] were the first to make measurements with time delay. Exhaustive measurements of the correlation between longitudinal velocity fluctuations in the turbulent boundary layer were made. It was discovered that the lines of maximum correlation at optimum time delay traveled outward from the surface at an angle of approximately

2° with the streamlines. Grant[2] has pointed out that such lines may represent the average particle paths, as viewed in a laboratory frame of reference, in the mixing jets suggested by himself. However, Favre found the longitudinal scale of the correlation at zero time delay to be three to four times the scale found by Grant. The cause of this discrepancy is unknown at the present time.

These measurements by Townsend, Grant, and Favre have made it clear that there is a certain amount of order in the eddy structure of the turbulent boundary layer.

More recently, the study of wall pressure fluctuations beneath the turbulent boundary layer has been undertaken. Experimental measurements of wall pressure intensity, power spectral density, and correlation have been obtained by many investigators. The results are summarized and compared in the paper by Willmarth and Wooldridge[5] which gives an account of a recent experimental investigation of the wall pressure beneath a thick turbulent boundary layer. This investigation established that the longitudinal and transverse scales of the pressure disturbance on the wall are nearly equal. The pressure fluctuations are found to be convected downstream at $0.83\ U_\infty$ and it is found that a disturbance of a given wavelength decays after traveling approximately six wavelengths.

In view of the previous velocity and wall pressure measurements described above, it was decided to measure the correlation between the fluctuating velocity and the fluctuating wall pressure to obtain additional knowledge about the structure of the flow.

The only previous pressure-velocity correlation measurements reported in the literature are those of Kawamura.[6] Kawamura attempted to measure the correlation between the wall pressure fluctuation and the longitudinal velocity fluctuation at zero time delay and zero longitudinal spacing between the points of measurement. The results do not agree with the present work for reasons which are not definitely known. The discrepancy may be due to the low signal-to-noise ratio reported by Kawamura, to the limitations of his pressure-measuring device, or to the influence of his trip.

The present investigation was carried out in a 5-in. thick turbulent boundary layer flow which was assumed to be incompressible. The ratios of pressure transducer diameter and hot wire length to boundary layer thickness were approximately 1:30 and 1:100 respectively, allowing a study of the detailed structure of the fluctuations in the layer.

II. EXPERIMENTAL APPARATUS AND PROCEDURE

A. WIND TUNNEL FACILITY

The experiments were carried out in the boundary layer on the floor of the 5 by 7 ft low speed wind tunnel facility at the Aeronautical Engineering Laboratories, The University of Michigan.

A schematic diagram showing the general lay-out is given in Fig. 1. Natural transition took place in the contraction section and no tripping device was required to make the boundary layer fully turbulent. A varnished and waxed sheet of masonite extending 14 ft upstream from the point of measurement was installed to make the wall aerodynamically smooth. In order to eliminate the undesirable effects of wind tunnel vibration, measurements were made on a 1-in. thick smooth (oil-lapped) steel plate, 20 in. in diameter and mounted on a heavy pedestal, which was inserted flush with the floor. The 1/16 in. gap which was allowed between the plate and the wind tunnel floor was sealed on the outside of the tunnel with a strip of rubber. The mounting pedestal was vibration-isolated from the floor by means of rubber shock pads. Holes were drilled in the plate to accept the pressure crystal assembly; holes not in use at any given time were filled with brass plugs which were fitted within $\pm$ 0.001 in. of the surface.

B. INSTRUMENTATION

The fluctuating wall pressure was measured with a 0.163 in. diam lead-zirconate crystal mounted in a brass body which was supported in the

steel plate by rubber O-rings. A schematic diagram of the transducer installation is shown in Fig. 2. The transducer was connected through a low-noise cable to a low-noise preamplifier having a cathode follower input with an input impedance of 1.2×10^8 ohms. The crystal capacity was 285 micro-microfarads, allowing a low frequency response down to approximately 5 cps. The gain of the preamplifier was approximately 50; it was followed by a two-stage amplifier which gave the entire system a maximum gain of 100,000. The bandwidth of the amplifier circuitry was adjustable between 1 cps and 160 kc.

The fluctuating velocities were measured with constant current hot wire equipment manufactured by Shapiro and Edwards. The frequency response of the uncompensated amplifier was flat from 0.13 cycles to 320 kilocycles. Adjustable filters in the amplifier were used to cut out frequencies above and below the range needed in the experiments to eliminate unnecessary noise. Tungsten wires 0.0002 in. in diam and approximately 0.050 in. long were attached to the supports by the usual method of copper plating and soldering. The time constant of the wires was approximately 0.40 msec. The compensation required to correct for the time lag of the wires was determined by the square wave method and accomplished by a resistance-capacitance network in the amplifier. No wire length corrections were applied to any of the data since the microscale of the turbulence near the wall was calculated from the measured spectra and found to be approximately twice the hot wire length. Moreover, the

upper frequency limit on the tape recorder described below limits the smallest eddy which can be studied to a scale of approximately twice the hot wire length.

In the inner 0.2 of the boundary layer a micrometer screw was used to position the hot wire probe. For the closest spacing to the wall, 0.050 in., the probe was located by measuring the distance between itself and its surface reflection for greater accuracy. At $y/\delta > 0.2$ the probe position was measured with an ordinary scale. A drawing of the hot wire probe for the closest spacing to the pressure transducer is also shown in Fig. 2.

The signals from the pressure and velocity transducers were recorded on a three-channel Ampex Model FR-1100 magnetic tape recorder which utilized 1/2-in. wide tape traveling at 60 in./sec. This recorder has a bandwidth extending from d-c to 10 kc which provided the limiting upper frequency for the measurements. A special play-back unit was designed for the recorder with one movable head to allow the introduction of time delay between a pair of signals. The smallest incremental time delay which could be set was 0.017 msec.

The correlator used in the measurement of the space-time correlations worked on the mean-square principle. A thermocouple was used to measure the mean-square values of each of the two signals to be correlated, of their sum, and of their difference. The sum was obtained from a simple resistive summing circuit built into the apparatus, and the difference was obtained by first sending one signal through an electronic phase in-

verter and then into the summing circuit. A provision for external filtering of the signal going to the thermocouple allowed the measurement of correlations in adjustable frequency bands; a Krohn-Hite Model 310-AB filter was used for this purpose. The output from the thermocouple was measured on a Sensitive Research d-c millivoltmeter having a time constant of 3 sec.

The spectral measurements were made using a fixed band-pass General Radio Model 736-A wave analyzer of the heterodyne type. The thermocouple circuitry in the correlator described above was used to obtain the mean-square value of the fluctuating output from the wave analyzer. Root-mean-square measurements were made with a Ballantine Model 320 true rms meter. Electrical signals were monitored with a DuMont Model 322-A dual-beam oscilloscope.

For the measurements of the correlation of pressure with velocity derivative, the velocity signal from the tape recorder was fed into a simple resistance-capacitance differentiating network having a linear response up to 10 kc. The attenuated output was amplified and fed into the correlator.

III. EXPERIMENTAL ENVIRONMENT

A. EXTRANEOUS DISTURBANCES

The accuracy of the measurements to be reported herein will be affected by the extraneous disturbances which are present. These include the vibration of the measuring apparatus, the sound field in the wind tunnel, the free stream turbulence level, and the mean flow conditions in the boundary layer. A comprehensive discussion of the sound measurements and flow visualization studies which were carried out is given in Ref. 5. A short summary of the results will be given here.

A check on the effectiveness of the vibration isolation of the mounting showed that the energy which was present because of vibration amounted to less than 1/100 of the energy in the turbulent pressure fluctuations and less than 1/100 of the energy in the turbulent velocity fluctuations near the edge of the boundary layer.

The sound field in the test section was first measured by a pressure transducer located on the stagnation line of an airfoil-shaped body exposed to the free stream. The spectrum of the stagnation pressure fluctuations had peaks at 135 and 200 cps. The wall pressure correlation measurements described in Ref. 5 which were made later showed a small peak at negative time delay which was caused by sound propagating upstream. From these data it was finally determined that the sound energy amounted to approximately 1/20 of the energy in the turbulent wall pressure fluctuations. The mean square velocity fluctuations associated with

the sound would amount to less than 5/1000 of the mean-square turbulent fluctuations near the edge of the boundary layer.

The settling chamber of the wind tunnel contains four turbulence damping screens. The free-stream turbulence level in the test section increases with velocity and has been measured at 50, 100, and 150 ft/sec. Extrapolation of the data to the 200 ft/sec speed used in this experiment results in a value of $\frac{\sqrt{\overline{u^2}}}{U_\infty} = 6 \times 10^{-4}$ for the turbulence level of the axial velocity component. The level of the transverse velocity component is approximately three times the level of the axial component.

Large-scale flow disturbances in the test section boundary layer were first discovered during the measurements of the wall pressure spectra which are described below. The entire wind tunnel, with the exception of the test section, is exposed to the weather. Heat transfer through the steel walls from sunshine produced a density stratification near the walls which in turn produced vorticity when accelerated into the test section. Observations of the streamlines on the concave surface of the contraction section showed large scale oscillations which were swept into the test section. It is believed that the large-scale disturbances observed in the test section are caused by a combination of the Taylor-Goertler boundary layer instability on the concave walls of the contraction and the density stratification.

B. PROPERTIES OF THE TURBULENT BOUNDARY LAYER USED IN THE INVESTIGATION

All measurements were made with natural transition in the boundary

layer which occurred approximately 24 ft ahead of the measuring point.

1. Mean Velocity Profiles.—The mean velocity profiles were measured with a total head tube; the static pressure was measured on the wall. No correction was made for the effect of turbulence on the mean values. Since the data presented in this report were taken over a period of time when the ambient temperature changed by some 20°, velocity profiles were taken at the extremes of temperature. The results were plotted on a non-dimensional basis in Fig. 3. The wall friction velocity was obtained from a measurement of the wall shear stress with a Stanton tube using the calibration results reported by Gadd.[8] Also shown in Fig. 3 is the ideal turbulent boundary layer profile of Coles.[9]

The properties of the measured boundary layer profile are tabulated in Table I together with the properties of Coles' ideal boundary layer at the same value of R_θ, the Reynolds number based on momentum thickness. Figure 3 and Table I show that there is satisfactory agreement with the ideal case.

TABLE I

COMPARISON OF BOUNDARY LAYER PARAMETERS WITH
COLES' IDEAL TURBULENT BOUNDARY LAYER PARAMETERS

T	U_∞	R_θ	δ	δ^*	θ	δ^*/θ	U_τ/U_∞	R	Remarks
67	204	38,000	0.42	0.041	0.0315	1.30	0.0326	3.1×10^7	Present investigation.
		38,000				1.30	0.0318	3.2×10^7	Coles' ideal boundary layer based on same R_θ.
45	203	43,000	0.42	0.041	0.0315	1.30	0.0325	3.85×10^7	Present investigation.
		43,000				1.295	0.0315	4.0×10^7	Coles' ideal boundary layer based on same R_θ.

2. Wall Pressure Spectrum.—The non-dimensional spectrum of the wall pressure is shown in Fig. 4. The data were always repeatable for $\frac{\omega\delta^*}{U_\infty} > 0.13$, but were not repeatable for $\frac{\omega\delta^*}{U_\infty} < 0.13$ ($f < 105$ cps). The results varied with the amount of heat transfer to the tunnel by sunlight. This variation is believed to be caused by the large-scale disturbances which arise from the density stratification discussed earlier in Section III-A.

In the measurements of mean-square pressure and velocity and space-time correlation of pressure with velocity the Krohn-Hite filter has been used to reject all frequencies below $\frac{\omega\delta^*}{U_\infty} = 0.13$. The upper limit on the frequency, $\frac{\omega\delta^*}{U_\infty} = 12.5$, was provided by the tape recorder response.

It is shown by the pressure-velocity correlation measurements reported in Section IV that the disturbances at any height in the boundary layer are convected at the local mean speed. At the closest spacing of the hot wire to the wall, 0.050 in., the local speed is approximately $0.58\ U_\infty$. Since the boundary layer thickness is 0.42 ft, disturbances convected at this speed which produce pressure fluctuations at $\frac{\omega\delta^*}{U_\infty} = 0.13$ have a wavelength of 2.78. Hence, even with filtering information can be obtained about eddies whose scale is at least 2-1/2 times the boundary layer thickness.

The root-mean-square value of the wall pressure fluctuation was 2.19 times the wall shear stress and 4.7×10^{-3} times the free stream dynamic pressure.

3. Velocity Intensity Profiles.—The intensity profiles of the ve-

locity fluctuations measured in the frequency band $0.13 < \frac{\omega\delta^*}{U_\infty} < 12.5$ are shown in Fig. 5. A comparison with the work of Klebanoff[10] shows that in the present case there are higher intensity levels in the inner half of the boundary layer and lower levels in the outer half of the layer for all three turbulence components. However, there are two main differences in the experimental conditions. In the present investigation there was natural transition of the boundary layer whereas Klebanoff used sandpaper roughness on the leading edge of his plate to trip the boundary layer. Also, the Reynolds number based on momentum thickness in the present experiment is approximately six times as large as Klebanoff's value. It should be noted that Klebanoff and Diehl[11] measured the u intensity profile in 1952 under the same operating conditions as those of Klebanoff[10] in 1955 and found values as much as 30% higher. Accordingly, it is believed that the intensity profiles of the turbulence in the boundary layer which are measured in any given case will be affected by the tripping device, if any, which is used and will depend upon the value of the Reynolds number in some unknown way. This is supported by the measurements of Ref. 5 which showed that either wall roughness or a boundary layer trip acted to increase the wall pressure intensity.

The intensity profile of the longitudinal derivative of the velocity fluctuation normal to the wall is shown for the inner half of the boundary layer in Fig. 6. A comparison with the data of Klebanoff[10] shows that the present results are approximately 2-1/2 times as large near the wall and 1-1/2 times as large near the center of the layer. It is believed

that this discrepancy is also due to either the boundary layer trip used by Klebanoff or the difference in Reynolds number.

4. Velocity Spectra.—The frequency spectra of the u and v velocity fluctuations which were measured directly with the wave analyzer have been converted to wave number spectra by assuming that the disturbance at any height is convected at the local mean speed and decays slowly. In this case the wave number is defined by

$$k = \frac{\omega}{U} \tag{1}$$

and the relation

$$E(k) = UE(\omega) \tag{2}$$

holds. These spectra which are shown in Figs. 7 and 8 are normalized to have unit area above $\frac{\omega\delta^*}{U_\infty} = 0.13$; the values of $\frac{\omega\delta^*}{U}$ corresponding to this are marked by the flagged point on each curve.

The non-dimensional u spectra, $\frac{UE_u(\omega)}{\delta^*}$, scale with the local non-dimensional wave number, $k\delta^* = \frac{\omega\delta^*}{U}$, except for the spectrum at the closest spacing to the wall at large wave number. This result implies that the disturbances in the frequency band under consideration are convected at the local mean speed. Moreover, the disturbances must be decaying slowly with time in this frequency band since only in the case of a completely frozen flow with no decay would the u spectra collapse perfectly into one universal curve. The spectrum near the wall at large wave number deviates from the other spectra because the small scale disturbances which are

relatively abundant near the wall decay relatively rapidly.

These data can be compared with the velocity-velocity correlation data obtained by others. The wave number spectral density, $E_u(k)$, is the transform of the longitudinal spatial correlation of the u velocity component; i.e.,

$$E_u(k) = \frac{\overline{u^2}}{\pi} \int_0^\infty R_{uu}(x_1) \cos kx_1 dx_1. \qquad (3)$$

If $E_u(k)$ is a function of k only, as the present data shows, then $R_{uu}(x_1)$ must be a universal function which is independent of the height in the boundary layer. Hinze[7] reports that the shape of the correlation curves $R_{uu}(x_1)$ measured by many investigators (see, e.g., Grant[2]) is independent of height except near $x_1 = 0$. The shape of $R_{uu}(x_1)$ near $x_1 = 0$ is governed by the behavior of the spectrum at large wave number (see Hinze[7]) and the non-uniform behavior of R_{uu} in this region is believed to be caused by the decay of the large wave number (small scale) fluctuations. For the same reason the spectral curves of $E_u(k)$ must separate at high wave number. The upper frequency in the present investigation was limited by the tape recorder response, and the data does not extend to a high enough wave number to show this effect. However, the separation at high wave number is shown by the data obtained by Klebanoff[10] who obtained measurements at frequencies higher than those studied in the present investigation.

In the outer half of the boundary layer, Klebanoff's u spectra in the frequency band corresponding to the present measurements also scaled

with the wave number based on the local velocity. In the inner half of the layer, however, the spectral curves were separated. The normalized curves showed relatively more high frequency energy near the wall. It is not known at this time whether this disagreement with the present data is an effect of the different Reynolds number or of the trip which was used by Klebanoff. However, the power dependence on non-dimensional wave number of the present spectral measurements agrees well with the power dependence found by Klebanoff.

The normalized v spectra shown in Fig. 7 do not scale with the wave number based on local velocity. Equivalent behavior is found by other investigators (see, e.g., Grant[2]) who have measured the longitudinal correlation of the u velocity and found the shape of $R_{uu}(x_1)$ to depend upon the height in the layer.* Therefore, it cannot be determined from the spectral curves whether or not the v disturbance is also convected at the local speed. However, the measurements of correlation between pressure and velocity which are presented in Section IV establish that this is the case.

The v spectra at the two points farthest from the wall exhibit humps near $\frac{\omega\delta^*}{U} = 0.4$. It is believed that these anomalies in the v spectra are caused by the large-scale extraneous disturbances discussed in Section III-A. Evidence to support this conclusion was obtained during

*These results imply that the v velocity fluctuation near the wall decays at a faster rate than the u velocity fluctuation in this region. This finding agrees with the results of the pressure-velocity correlation measurements described in Section IV which show that near the wall the R_{pv} correlation decays faster than the R_{pu} correlation.

measurements of the pressure-velocity correlations and is reported in Section IV.

IV. SPACE-TIME CORRELATION OF PRESSURE-VELOCITY

The fluctuating wall pressure and the fluctuating velocities in the boundary layer are stationary random functions of time and position. The pressure-velocity cross-correlation coefficients which have been measured are defined by

$$R_{pu}(x_1,x_2,x_3;\tau) = \frac{\overline{p(x,y,z;t)u(x+x_1,y+x_2,z+x_3;t+\tau)}}{\sqrt{\overline{p^2}(x,y,z;t)}\sqrt{\overline{u^2}(x+x_1,y+x_2,z+x_3;t)}} \qquad (4)$$

and

$$R_{pv}(x_1,x_2,x_3;\tau) = \frac{\overline{p(x,y,z;t)v(x+x_1,y+x_2,z+x_3;t+\tau)}}{\sqrt{\overline{p^2}(x,y,z;t)}\sqrt{\overline{v^2}(x+x_1,y+x_2,z+x_3;t)}} \qquad (5)$$

The experimental measurements are shown in Figs. 9 through 26 as functions of the non-dimensional time delay $\frac{U_\infty(\tau-\tau')}{\delta^*}$. The shift of the origin on the time delay axis, given by $\frac{U_\infty\tau'}{\delta^*}$, is computed at each value of $\frac{x_2}{\delta^*}$ by dividing the longitudinal spacing $\frac{x_1}{\delta^*}$ by the non-dimensional local mean speed $\frac{U}{U_\infty}$. A vertical line on each curve shows the true origin $\frac{U_\infty\tau}{\delta^*} = 0$.

A. ERRORS IN THE MEASUREMENTS

The averages involved in the computation of the correlation coefficients were obtained by visual observation of the output meter reading. Since the meter had a time constant of 3 sec, the fluctuations in the needle reading were small and the probable error in the correlation arising from this source is estimated to be ± 5% of the maximum value.

It was pointed out earlier in Section III-B that it was necessary to filter out the low frequencies, $\frac{\omega\delta^*}{U_\infty} < 0.13$. Such filtering will change the cross-correlation coefficient from that which would be measured if there were no filtering. The correlation will be changed in two ways:

1. the filter acts directly to destroy the correlation in the frequency band below its cut-off point, and
2. the filter acts indirectly to boost the value of the correlation coefficient at all values of time delay by reducing the magnitude of the denominator.

To estimate the amount of correlation caused by convected eddies which is destroyed by the filter, it is assumed that the wave number cross-spectral density is a slowly-varying function of time in a reference frame moving at the convection speed. In this frame the value of the spectrum below the wave number corresponding to the filter cut-off frequency is assumed to be constant and equal to the value at the cut-off frequency.

An analysis made by proceeding on this basis is given in the appendix. The results of this analysis show that the direct effect of the filtering changes the correlation curves most near their tails. This is to be expected since at large time delay the high frequency (small scale) velocity fluctuations have decayed, making the low frequency (large scale) fluctuations relatively more important. The filter effect also increases with distance from the wall since low frequency fluctuations become increasingly important in the correlation measurement as this distance increases. In no case, however, is the amount of correlation coefficient destroyed by

the filter larger than 10% of the peak value.

The indirect effect of the filtering is to increase the measured values of R_{pu} by approximately 15% and those of R_{pv} by approximately 8% above the values which would have been measured with no filtering.

The boundary layer should be homogeneous in the z-direction; one would expect R_{pu} and R_{pv} to be symmetric about $x_3 = 0$ and R_{pw} to be zero. Symmetry about $x_3 = 0$ was found in the measurements; see, for example, Fig. 27. The cross-correlation coefficient R_{pw}, defined in a similar manner to R_{pu} and R_{pv}, was measured at various values of $\frac{x_2}{\delta^*}$ in the two frequency bands $0.13 < \frac{\omega\delta^*}{U_\infty} < 12.5$ (the usual band) and $0.38 < \frac{\omega\delta^*}{U_\infty} < 12.5$. Some typical results are shown in Fig. 28.

The measured correlation is small but definitely not zero, and has approximately the same scale throughout the boundary layer. The transverse scale across the stream is only about 0.1 of the longitudinal scale along the stream. Filtering of the frequencies below 300 cps ($\frac{\omega\delta^*}{U_\infty} < 0.38$) destroys most of the correlation. The reason for the lack of symmetry about $\frac{U_\infty \tau}{\delta^*} = 0$ is unknown at the present time.

It is believed that this R_{pw} correlation is caused by a vortex whose axis is in the longitudinal direction and near the edge of the boundary layer. This vortex is believed to be a result of the Taylor-Goertler instability and the density stratification which were discussed earlier in Section III-A. Unfortunately, no measurements of R_{pw} were made at different cross-stream locations; such measurements might have shed more light on the nature of the inhomogeneity.

The filter cut-off frequency $\frac{\omega\delta^*}{U_\infty} = 0.38$ above which the R_{pw} correlation is nearly gone corresponds closely to the frequency at which the v spectra exhibited a peak. It is believed that both phenomena are connected with the extraneous vortex disturbance. In this case the value of the R_{pv} correlation will also be affected near the tails of the curve where the low frequencies make a sizable contribution, but this effect is believed to be small.

In view of these results the measurements are believed to present a valid description of the fluctuating flow field which is produced by the convected disturbances.

B. RESULTS OF THE MEASUREMENTS

The convection speed, U_c, of the disturbance which gives rise to the pressure-velocity correlation is defined as the speed of travel of the center of the disturbance where the correlation is zero. Examination of Figs. 9 through 26 shows that at any height in the boundary layer this convection speed is equal to the local mean speed; i.e.,

$$U_c = U. \tag{6}$$

When normalized on local root-mean-square values of the fluctuating velocity, the pressure-velocity correlation coefficients near the edge of the boundary layer have approximately the same magnitude as those near the wall. When the correlation coefficients are normalized on the values of the fluctuating velocities at one point, however, the magnitude of the

correlation near the edge of the layer is only 0.01 of the magnitude near the wall.

It is shown in Section V that the wall pressure fluctuations are produced by the interaction of the longitudinal derivative of the velocity fluctuation normal to the wall with the mean shear in a region close to the wall. It is believed that the wall pressure is correlated with the fluctuating velocities far from the wall because these velocities are correlated with the velocities near the wall which do produce the pressure.

One might hypothesize that the fluctuating velocities near the wall which are involved in the production of the wall pressure are caused by those eddies of various sizes which are in contact with a layer of fluid very close to the wall. These eddies extend outward into the stream varying distances and the largest scale of such eddies is probably of the order of the boundary layer thickness. The values of the correlation coefficients based on the root-mean-square velocity fluctuations at one point decrease with increasing distance from the wall because less and less of the eddy field is seen by the hot wire as this distance increases. A further discussion of this hypothesis is given in Section VII.

Figures 9 through 26 also show that the pressure-velocity correlations R_{pu} and R_{pv} at any height have nearly equal magnitude and opposite algebraic signs except at large values of negative time delay where both are small and negative. This result implies that the velocity disturbance which is correlated with the wall pressure also acts to create at least part of the turbulent shear. Further investigation is needed, however,

before the exact relationship between the turbulent shear and the fluctuating wall pressure will be known.

V. SPACE-TIME CORRELATION OF PRESSURE WITH THE TIME DERIVATIVE OF THE VELOCITY FLUCTUATION NORMAL TO THE WALL

In incompressible flow the equation of continuity can be combined with the equations of momentum to give a Poisson equation for the pressure,

$$\nabla^2 \mathcal{P} = - \rho \frac{\partial \mathcal{U}_i}{\partial x_j} \frac{\partial \mathcal{U}_j}{\partial x_i}, \tag{7}$$

in tensor notation. $\mathcal{P}$ and $\mathcal{U}$ represent the total pressure and total velocity respectively. The equation for the fluctuating pressure can be obtained by setting each flow quantity equal to a mean value plus a fluctuation, expanding the derivative, and subtracting the equation for the mean pressure from the total equation. Kraichnan[12] has shown that the dominant term in the equation for the fluctuating pressure is

$$\nabla_p^2 = - 2\rho \frac{\partial U}{\partial y} \frac{\partial v}{\partial x}. \tag{8}$$

Since the wall pressure p is produced by the values of the derivative $\frac{\partial v}{\partial x}$ which exist throughout the velocity field, a measurement of the correlation of p with $\frac{\partial v}{\partial x}$ will show which regions of the fluctuating velocity field do not contribute to the wall pressure. The cross-correlation coefficient R_{pv_x}, where $v_x = \frac{\partial v}{\partial x}$, is defined by

$$R_{pv_x} = \frac{\overline{p(x,y,z;t) v_x(x+x_1, y+x_2, z+x_3; t+\tau)}}{\sqrt{\overline{p^2}(x,y,z;t)} \sqrt{\overline{v_x^2}\,(x+x_1, y+x_2, z+x_3; t)}} \tag{9}$$

This correlation is difficult to measure experimentally. However, if the velocity disturbance is convected past the hot wire with little distortion (see Section VI), the equation

$$\frac{\partial v}{\partial x} = - \frac{1}{U_c} \frac{\partial v}{\partial t} \tag{10}$$

can be used to relate space and time derivatives. In this case

$$R_{pv_x} = - R_{p\dot{v}}$$

where $\dot{v} = \frac{\partial v}{\partial t}$. The cross-correlation coefficient

$$R_{p\dot{v}} = \frac{\overline{p(x,y,z;t)\dot{v}(x+x_1,y+x_2,z+x_3;t+\tau)}}{\sqrt{\overline{p^2}\,(x,y,z;t)}\sqrt{\overline{\dot{v}^2}\,(x+x_1,y+x_2,z+x_3;t)}} \tag{11}$$

can be easily measured by differentiating the velocity signal electrically and correlating the result with the wall pressure.

The measured values of this correlation coefficient are shown in Figs. 29 through 31, again plotted versus the non-dimensional time delay $\frac{U_\infty(\tau-\tau')}{\delta^*}$. A vertical line on each curve for $\frac{x_1}{\delta^*} > 0$ shows the true origin $\frac{U_\infty \tau}{\delta^*} = 0$. These measurements again illustrate the fact that the convection speed of the velocity disturbance which is correlated with the wall pressure is equal to the local mean speed.

A very simple mathematical relationship exists between the correlation coefficients $R_{p\dot{v}}$ and R_{pv}:

$$R_{p\dot{v}} = \frac{\sqrt{\overline{v^2}}}{\sqrt{\overline{\dot{v}^2}}} \frac{\partial}{\partial \tau} R_{pv}. \tag{12}$$

The decrease in the slope of R_{pv} as the distance from the wall increases means that velocity fluctuations far from the wall have comparatively little effect in producing pressure fluctuations at the wall. However, these velocity fluctuations are correlated with the wall pressure because they are correlated with the velocity fluctuations near the surface which do produce the pressure (see Section IV-B).

A. ERRORS IN THE MEASUREMENTS

As in the measurement of the pressure-velocity correlations, the probable errors which arise from the averaging process are estimated to be ± 5% of the maximum value of the correlation.

During the measurement of $R_{p\dot{v}}$ the frequencies corresponding to $\frac{\omega\delta^*}{U_\infty} < 0.13$ were filtered out as before. An analysis of the low-frequency filter effect, based on the assumption of a constant wave number spectral density below the filter cut-off point as before, is given in the appendix. This direct filter effect of destroying the correlation at low frequencies is found to be negligible.

The indirect effect of the filter reduces the size of the normalization factors at all values of time delay. The measured values of $R_{p\dot{v}}$ are increased approximately 6% by the filtering. This error is comparable to those occurring in the pressure and velocity measurements.

B. RESULTS OF THE MEASUREMENTS

The curves of $R_{p\dot{v}}$ given in Figs. 29 through 31 are normalized on the local values of the fluctuating velocity field. When normalized on

the velocity at one point, the data exhibits the same general behavior. A maximum in the peak value of the correlation is reached at a short distance from the wall; the peak value then decreases with increasing distance from the wall and becomes negligible for $\frac{x_2}{\delta^*} > 4.08$.

The convection speed of the disturbance which gives rise to $R_{p\dot{v}}$ is the local mean speed in the boundary layer as pointed out at the beginning of this section. On the other hand the convection speed of the wall pressure disturbance has been determined in Ref. 5 to vary from $0.56\ U_\infty$ to $0.83\ U_\infty$ as the spacing between the measuring points is increased. Since the wall pressure fluctuation, p, is an integral over all space of the velocity fluctuation derivative, $\frac{\partial v}{\partial x}$, the final value of the convection speed of the wall pressure disturbance which is attained at large transducer spacing should not exceed the local speed in the boundary layer where $R_{p\dot{v}}$ becomes negligible. At $\frac{x_2}{\delta^*} = 4.08$ the local speed is approximately 0.9 of the free-stream speed and the restriction on the convection speed is satisfied. The speed $0.83\ U_\infty$ occurs as the local speed in the boundary layer at $\frac{y}{\delta^*} = 2.25$ ($\frac{y}{\delta} \cong 0.22$).

VI. CONTOURS OF CONSTANT CORRELATION

The statistical structure of the turbulent velocity field which creates the turbulent wall pressure is shown by the spatial correlation contours of R_{pu}, R_{pv}, and $R_{p\dot{v}}$. A direct measurement of enough data points to allow the construction of these contours would be extremely time consuming; furthermore, it was found during the experimental measurements that interference effects between the hot wire probe and the pressure transducer made it impossible to obtain reliable data with the hot wire ahead of the pressure transducer, $x_1 < 0$. The measurements for $x_1 > 0$ show that the rate of decay is slow and that the convection speed is the local speed as pointed out in Section IV. Hence, it is possible to obtain approximate spatial correlation contours from the measured time-delay correlations at zero longitudinal separation by using the convection transformation

$$\frac{x_1}{\delta^*} = -\frac{U_\infty \tau}{\delta^*} \frac{U}{U_\infty} \tag{13}$$

The correlation contours obtained by the use of this transformation are shown in Figs. 32 through 40 where the origin of the coordinate system is located at the point where the wall pressure was measured. The values of the correlation coefficients which are shown have been standardized using the root-mean-square values of the velocity fluctuations at $y/\delta^* = 0.51$ as normalization factors; i.e., at any position

$$R'_{pu} = R_{pu}\sqrt{\frac{\overline{u^2}_{local}}{\overline{u^2}_{0.51}}}$$

$$R'_{pv} = R_{pv}\sqrt{\frac{\overline{v^2}_{local}}{\overline{v^2}_{0.51}}} \qquad (14)$$

$$R'_{\dot{p}v} = R_{\dot{p}v}\sqrt{\frac{\overline{\dot{v}^2}_{local}}{\overline{\dot{v}^2}_{0.51}}}$$

The ratios of the root-mean-square velocities and velocity derivatives are obtained from the intensity profiles in Figs. 5 and 6.

A. ERRORS CAUSED BY THE CONVECTION HYPOTHESIS

The validity of the convection hypothesis clearly depends upon the spatial rate of change (growth or decay) of the velocity disturbance. The velocity spectral measurements reported in Section III-B-4 above show that the u velocity disturbance decays slowly and lend support to this hypothesis.

The amount of error introduced can be determined at those values of $\frac{x_1}{\delta^*}$ for which data were taken by comparing the measured values of the spatial correlation at zero time delay with the values predicted by the convection hypothesis.

These data show that the use of the transformation is most in error near the wall. This is to be expected since the high frequency (small scale) velocity fluctuations which make a measurable contribution to the correlation near the wall decay more rapidly than the lower frequency fluctuations farther from the wall. The u velocity spectra discussed

previously in Section III-B also tended to show that the hypothesis of convection is most in error near the wall at the high frequency end of the spectrum.

The measurements also show that the error introduced in R_{pv} by the convection transformation near the wall is greater than that introduced in R_{pu}. This effect is also apparent in the velocity correlation data obtained by Grant[2] which shows that correlation of the velocity component normal to the surface decays much faster than the correlation of the longitudinal component parallel to the surface (see also Section III-B-4). The reason for this behavior is not known at the present time.

The maximum error in the correlation near the peak value of R_{pv} is approximately ± 20% of the peak value near the wall; for $y/\delta^* > 0.2$ the error is ± 10% or less. The errors in R_{pu} near the peak values are ± 10% or less of the peak value for all heights in the boundary layer. A few points measured at large values of $\frac{x_1}{\delta^*}$ show that the errors in the tails of the curves for large time delay are also approximately ± 10% of the peak value.

Since $R_{p\dot{v}}$ is the derivative of R_{pv}, the error in $R_{p\dot{v}}$ near its peak value can be obtained by extrapolating the R_{pv} data which were measured at various values of $\frac{x_1}{\delta^*}$ to $\frac{x_1}{\delta^*} = 0$ and comparing the slope obtained to the slope predicted by the convection hypothesis. The results show that the error in $R_{p\dot{v}}$ is a maximum near the wall at $\frac{x_2}{\delta^*} = 0.1$ and is at most ± 30%. At all other spacings the error in $R_{p\dot{v}}$ is less than ± 10%.

B. THE STRUCTURE OF THE CORRELATION FIELDS

A few general remarks can be made about the shapes of the correlation contours. The contour curves of R_{pu} and R_{pv} in the x_1-x_2 plane (Figs. 32 and 35) show that the scale perpendicular to the wall is slightly larger downstream from the pressure transducer than upstream. This is also shown in the contours in the x_2-x_3 plane (Figs. 33 and 36). The R_{pv} contour curves in the x_1-x_3 plane (Fig. 37) show that near the wall the contours bend upstream. The $R_{p\dot{v}}$ contours (Figs. 38 through 40) are related to the R_{pv} contours through the differentiation noted previously. The region of negative $R_{p\dot{v}}$ (corresponding to positive R_{pv_x}) has a slightly larger scale in the transverse than in the longitudinal direction.

The spatial extent of the turbulent velocity field which is correlated with the wall pressure can be put on a quantitative basis by defining integral scales. The integral scales of R_{pu} and R_{pv} in the x_i-direction are defined to be

$$(\Lambda_{pu})_i = \frac{1}{|R_{pu}|_{max}} \int_{-\infty}^{\infty} \left| R_{pu}\left(\frac{x_i}{\delta^*}\right) \right| d\left(\frac{x_i}{\delta^*}\right)$$

$$(\Lambda_{pv})_i = \frac{1}{|R_{pv}|_{max}} \int_{-\infty}^{\infty} \left| R_{pv}\left(\frac{x_i}{\delta^*}\right) \right| d\left(\frac{x_i}{\delta^*}\right) \qquad (15)$$

For the scale normal to the wall the integration extends from zero to infinity.

Calculation of this basis shows that:

1. The longitudinal scales of R_{pu} and R_{pv} are approximately equal to the boundary layer thickness, δ, being slightly smaller near

the wall and slightly larger near the middle of the layer.

2. The transverse scales parallel to the wall and perpendicular to the mean velocity increase with distance from the wall and reach a maximum value of approximately 0.2δ at a height of approximately 0.2δ in the layer. Beyond this height the scales decrease.

3. The scales normal to the wall are a maximum at $x_3 = 0$. The scale of R_{pu} is approximately 0.2δ and that of R_{pv} is 0.3δ at $\frac{x_1}{\delta^*} = -1.25$; these scales are approximately 10% larger at $\frac{x_1}{\delta^*} = +1.25$.

These results demonstrate that the region of the velocity field which is correlated with the wall pressure is comparatively long in the longitudinal direction and narrow in the other two perpendicular directions.

A spatial scale for the velocity correlations measured by Grant[2] and Favre[3,4] can be defined by

$$\frac{(\Lambda_{uu})_i}{\delta^*} = 2 \int_0^\infty R_{uu}\left(\frac{x_i}{\delta^*}\right) d\left(\frac{x_i}{\delta^*}\right). \qquad (16)$$

Using this equation, Grant's longitudinal scale is calculated to be approximately 0.4δ and Favre's to be approximately 1.0δ. In the transverse direction both investigators find a scale of approximately 0.3δ. The reason for the discrepancy in the longitudinal scale is unknown at the present time but probably involves the differences in the tripping devices used in the two experiments.

These results show that even though a fundamentally different measurement is involved, the velocity-velocity correlation scales are of the

same order as the pressure-velocity correlation scales.

The spatial scales of $R_{p\dot{v}}$ are defined in a similar way to those of R_{pu} and R_{pv} by

$$\frac{(\Lambda_{p\dot{v}})_i}{\delta^*} = \frac{1}{|R_{p\dot{v}}|_{max}} \int_{-\infty}^{\infty} |R_{p\dot{v}}\left(\frac{x_i}{\delta^*}\right)| \, d\left(\frac{x_i}{\delta^*}\right) \tag{17}$$

These scales are smaller than the corresponding scales of the pressure-velocity correlations. Calculation shows that

1. The longitudinal scale is approximately 0.2δ.
2. The maximum transverse scale is approximately 0.15δ at a height of 0.1δ.
3. The scale normal to the wall, a maximum at $x_3 = 0$, is approximately 0.15δ at $x_1 = 0$.

A scale for the wall pressure correlation reported in Ref. 5 can be defined by

$$\frac{(\Lambda_{pp})_i}{\delta^*} = 2 \int_0^{\infty} R_{pp}\left(\frac{x_i}{\delta^*}\right) d\left(\frac{x_i}{\delta^*}\right) \tag{18}$$

The longitudinal scale of the pressure-pressure correlation calculated in this way is approximately 0.25δ; the transverse scale is slightly larger than this.

Hence, the integral scales of R_{pp} and $R_{p\dot{v}}$ are nearly the same. Since the wall pressure is an integral of the velocity derivative over all space, this result shows that the present data is consistent with the data obtained in Ref. 5.

The scale of $R_{p\dot{v}}$ normal to the wall is only about one-half of the

scale of R_{pv} normal to the wall. This lends support to the hypothesis (Section IV-B) that even though only the derivatives of the velocity fluctuations near the wall create the wall pressure, these velocity fluctuations are part of an eddy system which extends farther outward into the flow.

VII. VECTOR FIELD OF THE CORRELATIONS

The correlation vector field shown in Fig. 41 has been constructed with the origin at the pressure transducer such that:

1. the length of the vector at any point is given by $\sqrt{R_{pu}^2+R_{pv}^2}$, where the correlations are based on the local root-mean-square values of the velocity fluctuations, and
2. the direction of each vector, measured from the positive x_1-axis, is given by $\tan^{-1}\frac{R_{pv}}{R_{pu}}$ where the wall pressure pulse is assumed to be negative.

It is known that part of the velocity field which produces the fluctuating wall pressure is convected at the local speed in the boundary layer with a slow rate of decay. The wall pressure p depends upon the values of $\frac{\partial v}{\partial x}$ in the vicinity of the wall. The velocity fluctuations are caused by a collection of vortex filaments with random orientation. It is hypothesized that those filaments which lie along the x_3-direction make the major contribution to R_{pv} as the velocity field is convected along the wall, but it is admitted that further experiments are needed to clarify this point. Furthermore, it is known from the measurements of R_{pv_x} reported in Section V that only those filaments whose influence extends to the vicinity of the wall act to generate the wall pressure.

On this basis it is further hypothesized that the velocity field which is correlated with the wall pressure is generated by a system of eddies of all sizes which are in contact with a layer of fluid very close

to the wall (see also Section IV-B). The correlation vector field shown in Fig. 41 is believed to represent the velocity field which is generated by a superposition of these eddies. As pointed out above, the field was mapped by assuming the pressure pulse to be negative. The rotation of the vector field in Fig. 41 is then clockwise which is reasonable from a consideration of the mean shear.

There is some evidence in the R_{pv} and $R_{p\dot{v}}$ correlation contours in the x_1-x_3 plane (Figs. 37 and 40) that near the wall the vortex filaments which generate the vector field bend upstream.

Further experimental investigation is needed to positively confirm or deny the hypothesis of the hierarchy of eddies which is set forth here, but all of the present data support it.

VIII. CONCLUDING REMARKS

The main results of this experimental investigation can be summarized as follows:

1. Evidence has been accumulated that a boundary layer trip has a rather severe effect on the properties of turbulence in the boundary layer. From a study of the data of other investigators and a comparison with the present investigation, it is evident that a trip acts to increase the wall pressure intensity and the velocity intensity near the wall. The experiments of Grant[2] and Favre[3,4] show that the integral scale of the longitudinal velocity correlation is also affected by the trip used. It now appears that some features of the turbulent structure obtained in many of the previous investigations in tripped boundary layers were not always universal but were a function of the experimental conditions imposed by the tripping device.

The results of the present investigation with natural transition of the boundary layer are believed to be universal because no tripping device was required to make the boundary layer fully turbulent.

2. The convection speed of the velocity disturbance which is correlated with the wall pressure disturbance is the local mean speed.

3. The R_{pu} and R_{pv} correlation coefficients are of opposite sign. This implies that the part of the velocity field which is correlated with the wall pressure also acts to produce turbulent shear stress in the boundary layer.

4. The measurement of $R_{p\dot{v}}$ shows that most of the wall pressure is produced by velocity fluctuations near the surface.

5. Velocity fluctuations far from the wall are correlated with the wall pressure because they in turn are correlated with the velocity fluctuations near the wall which do produce the wall pressure.

6. Present measurements of the $R_{p\dot{v}}$ correlation show that the convection speed of the wall pressure disturbance should not exceed 0.9 U_∞, the local speed at $y/\delta \cong 0.4$. The measurements of Ref. 5 showed the value of this convection speed to be 0.83 U_∞ at large transducer spacing and the restriction is satisfied. The speed 0.83 U_∞ occurs in the boundary layer profile at $y/\delta \cong 0.22$.

7. The integral scales of R_{pu} and R_{pv} are approximately the same as the integral scales of R_{uu} measured by other investigators. The longitudinal scales of R_{pu} and R_{pv} are approximately equal to the boundary layer thickness, δ. The transverse scales are approximately 0.2δ and the scales normal to the plate are approximately 0.2δ and 0.3δ for R_{pu} and R_{pv} respectively.

8. A vector field of the pressure-velocity correlation data is presented. The hypothesis is made that this field represents the velocity field generated by a superposition of eddies of all sizes whose axes lie parallel to the wall and perpendicular to the mean velocity which are in contact with a layer of fluid near the wall.

APPENDIX

LOW-FREQUENCY FILTER EFFECT

LOW-FREQUENCY FILTER EFFECT

During the analysis of the experimental data it was found that it was necessary to filter out the low frequency energy, $\frac{\omega\delta^*}{U_\infty} < 0.13$. Here an expression will be derived for the amount of correlation in the frequency band below the cut-off point which is destroyed by the filtering. It is assumed that the wave number cross-spectral density in a frame of reference moving at the convection speed is a slowly varying function of time so that it can be approximated by a constant below the wave number corresponding to the filter cut-off frequency.

Take the Fourier transform of the cross-correlation coefficient R_{pv}, say, in one dimension in the fixed coordinate system.

$$F_{pv}(k_1,x_2,x_3;\tau) = \frac{1}{2\pi}\int_{-\infty}^{\infty} R_{pv}(x_1,x_2,x_3;\tau)e^{-ik_1x_1}dx_1 \qquad (1)$$

The inverse relation is

$$R_{pv}(x_1,x_2,x_3;\tau) = \int_{-\infty}^{\infty} F_{pv}(k_1,x_2,x_3;\tau)e^{ik_1x_1}dk_1 \qquad (2)$$

Let the coordinates in a reference frame moving at the local convection speed be denoted by (x_1',x_2',x_3'). Then the two coordinate systems are related by

$$\begin{aligned} x_1 &= x_1' + U_c\tau \\ x_2 &= x_2' \\ x_3 &= x_3' \end{aligned} \qquad (3)$$

In terms of the new coordinates

$$R_{pv}(x_1'+U_c\tau, x_2', x_3'; \tau) = \int_{-\infty}^{\infty} F_{pv}(k_1, x_2', x_3'; \tau) e^{ikU_c\tau} e^{ik_1 x_1'} dk_1 \qquad (4)$$

$$= \int_{-\infty}^{\infty} G_{pv}(k_1, x_2', x_3'; \tau) e^{ik_1 x_1'} dk_1 \qquad (5)$$

The last equation serves to define a new spectral function G_{pv} which is the transform of R_{pv} in the moving frame. Let

$$G_{pv} = \bar{U}_{pv} + i\,\bar{V}_{pv} \qquad (6)$$

Since R_{pv} is a real-valued function, $\bar{U}_{pv}$ and $\bar{V}_{pv}$ must be respectively even and odd in k_1, allowing the correlation function to be written as

$$\begin{aligned} R_{pv}(x_1'+U_c t, x_2', x_3'; \tau) &= 2\int_0^{\infty} \bar{U}_{pv}(k_1, x_2', x_3'; \tau) \cos k_1 x_1 dk_1 \\ &\quad - 2\int_0^{\infty} \bar{V}_{pv}(k_1, x_2', x_3'; \tau) \sin k_1 x_1 dk_1 \end{aligned} \qquad (7)$$

The filter acts to truncate the spectrum at some wave number $k_1 = K_1$. If it is assumed that $\bar{U}_{pv}$ and $\bar{V}_{pv}$ are constant below this wave number, one can write

$$\begin{aligned} \Delta R_{pv}(x_1'+U_c\tau, x_2', x_3'; \tau) &= 2\,\bar{U}_{pv}(K_1, x_2', x_3'; \tau) \int_0^{K_1} \cos k_1 x_1' dk_1 \\ &\quad - 2\,V_{pv}(K_1, x_2', x_3'; \tau) \int_0^{K_1} \sin k_1 x_1 dk_1 \qquad (8) \\ &= 2\,\bar{U}_{pv} \frac{\sin K_1 x_1'}{x_1'} - 2\,\bar{V}_{pv} \frac{1-\cos K_1 x_1'}{x_1'} \end{aligned}$$

This equation is the expression for that part of the cross-correlation coefficient which has been destroyed by the filtering process, under the assumption that the cross-spectral density is constant for wave numbers below K_1.

The formulas for the calculation of $\bar{U}_{pv}$ and $\bar{V}_{pv}$ at the wave number K_1 are

$$\bar{U}_{pv}(K_1,x_2',x_3';\tau) = \frac{1}{2\pi}\int_{-\infty}^{\infty} R_{pv}(x_1'+U_c\tau,x_2',x_3';\tau)\cos K_1x_1'dx_1' \tag{9}$$

$$\bar{V}_{pv}(K_1,x_2',x_3';\tau) = -\frac{1}{2\pi}\int_{-\infty}^{\infty} R_{pv}(x_1'+U_c\tau,x_2',x_3';\tau)\sin K_1x_1'dx_1' \tag{10}$$

Since the correlation R_{pv} has been measured in the time domain, the computation of the spectral densities can be simplified by transforming Eqs. (9) and (10) into the time domain.

If x_1, the distance between the transducers in the fixed frame of reference, is taken as a parametric constant, the wave number in the moving frame of reference can be related to the frequency by

$$k_1 = \frac{\omega}{U_c}$$

If ω_1, is the cut-off frequency of the filter,

$$K_1 = \frac{\omega_1}{U_c} \tag{11}$$

The coordinate transformation relating x_1 and x_1' is [from Eq. (3)]

$$x_1' = x_1 - U_c\tau; \tag{12}$$

for x_1 constant,

$$dx_1' = -U_c d\tau \tag{13}$$

Using Eqs. (11), (12), and (13), the expressions for $\bar{U}_{pv}$ and $\bar{V}_{pv}$ can now be written in terms of fixed coordinates and time delay as

$$\bar{U}_{pv}(x_1,x_2,x_3;\omega_1) = \frac{U_c}{2\pi}\int_{-\infty}^{\infty} R_{pv}(x_1,x_2,x_3;\tau)\cos\omega_1\left(\frac{x_1}{U_c}-\tau\right)d\tau \quad (14)$$

$$\bar{V}_{pv}(x_1,x_2,x_3;\omega_1) = -\frac{U_c}{2\pi}\int_{-\infty}^{\infty} R_{pv}(x_1,x_2,x_3;\tau)\sin\omega_1\left(\frac{x_1}{U_c}-\tau\right)d\tau \quad (15)$$

The expression for the increment in the correlation coefficient becomes

$$\Delta R_{pv}(x_1,x_2,x_3;\tau) = \frac{2}{U_c}U_{pv}(x_1,x_2,x_3;\omega_1)\frac{\sin\omega_1\left(\frac{x_1}{U_c}-\tau\right)}{\frac{x_1}{U_c}-\tau} - \frac{2}{U_c}V_{pv}(x_1,x_2,x_3;\omega_1)\frac{1-\cos\omega_1\left(\frac{x_1}{U_c}-\tau\right)}{\frac{x_1}{U_c}-\tau} \quad (16)$$

A similar analysis leads to an equation for ΔR_{pu} with $\bar{U}_{pv}$ and $\bar{V}_{pv}$ replaced by $\bar{U}_{pu}$ and $\bar{V}_{pu}$ respectively. Note that the hypothesis of convection which has been used leads to the conclusion that a constant wave number spectrum for $k_1 < K_1$ implies that the frequency spectrum is a constant for $\omega < \omega_1$.

The results of the calculation using (16) have been reported in Section IV-A.

The effect of the filtering on $R_{p\dot{v}}$ can be obtained by differentiation. One can write

$$\Delta R_{p\dot{v}} = \frac{\sqrt{\overline{v^2}}}{\sqrt{\overline{\dot{v}^2}}}\frac{d}{d\tau}\Delta R_{pv}$$

$$= \frac{\sqrt{\overline{v^2}}}{\sqrt{\overline{\dot{v}^2}}}\left\{\frac{2}{U_c}\bar{U}_{pv}\left[\frac{\sin\omega_1\left(\frac{x_1}{U_c}-\tau\right)}{\left(\frac{x_1}{U_c}-\tau\right)^2} - \frac{\omega_1\cos\omega_1\left(\frac{x_1}{U_c}-\tau\right)}{\frac{x_1}{U_c}-\tau}\right]\right. \quad (17)$$

$$\left. - \frac{2}{U_c}\bar{V}_{pv}\left[\frac{1-\cos\omega_1\left(\frac{x_1}{U_c}-\tau\right)}{\left(\frac{x_1}{U_c}-\tau\right)^2} - \frac{\omega_1\sin\omega_1\left(\frac{x_1}{U_c}-\tau\right)}{\frac{x_1}{U_c}-\tau}\right]\right\}$$

A direct calculation shows that $\Delta R_{p\dot{v}}$ is negligible in all cases.

REFERENCES

1. Townsend, A. A., "The Structure of the Turbulent Boundary Layer," Proc. Camb. Phil, Soc., 47, 1950, 375-395.

2. Grant, H. L., "The Large Eddies of Turbulent Motion," J. Fluid Mech., 4, 1958, 149-190.

3. Favre, A. J., J. J. Gaviglio, and R. Dumas, "Space-Time Double Correlations and Spectra in a Turbulent Boundary Layer," J. Fluid Mech., 2, 1957, 313-342.

4. Favre, A. J., J. J. Gaviglio, and R. Dumas, "Further Space-Time Correlations of Velocity in a Turbulent Boundary Layer," J. Fluid Mech., 3, 1958, 344-356.

5. Willmarth, W. W., and C. E. Wooldridge, "Measurements of the Fluctuating Pressure at the Wall Beneath a Thick Turbulent Boundary Layer," Univ. of Mich. ORA Report for ONR Contract No. Nonr 1224(30). Also submitted to J. Fluid Mech.

6. Kawamura, M., "Pressure-Velocity Correlation and Double Velocity Correlation in a Turbulent Boundary Layer Along a Flat Plate," J. Sci. Hiroshima Univ. Ser. A, 24, No. 2, 1960, 403-416.

7. Hinze, J. O., Turbulence, New York: McGraw-Hill Book Company, 1959, Chapter 1.

8. Gadd, G. E., "A Note on the Theory of the Stanton Tube," Brit. R. and M. 3147, 1960.

9. Coles, D., "Measurements in the Boundary Layer on a Smooth Flat Plate in Supersonic Flow. I. The Problem of the Turbulent Boundary Layer," Jet Prop. Lab Rep 20-69, 1953, or Z.A.M.P., V, 1954, 181.

10. Klebanoff, P. S., "Characteristics of Turbulence in a Boundary Layer With Zero Pressure Gradient," NACA Rep. 1247, 1955.

11. Klebanoff, P. S., and Z. W. Diehl, "Some Features of Artificially Thickened Fully Developed Turbulent Boundary Layers with Zero Pressure Gradient," NACA Rep. 1110. 1952.

12. Kraichnan, R. H., "Pressure Fluctuations in Turbulent Flow Over a Flat Plate," J. Acoust. Soc. Am., 28, No. 3, 1956, 378-390.

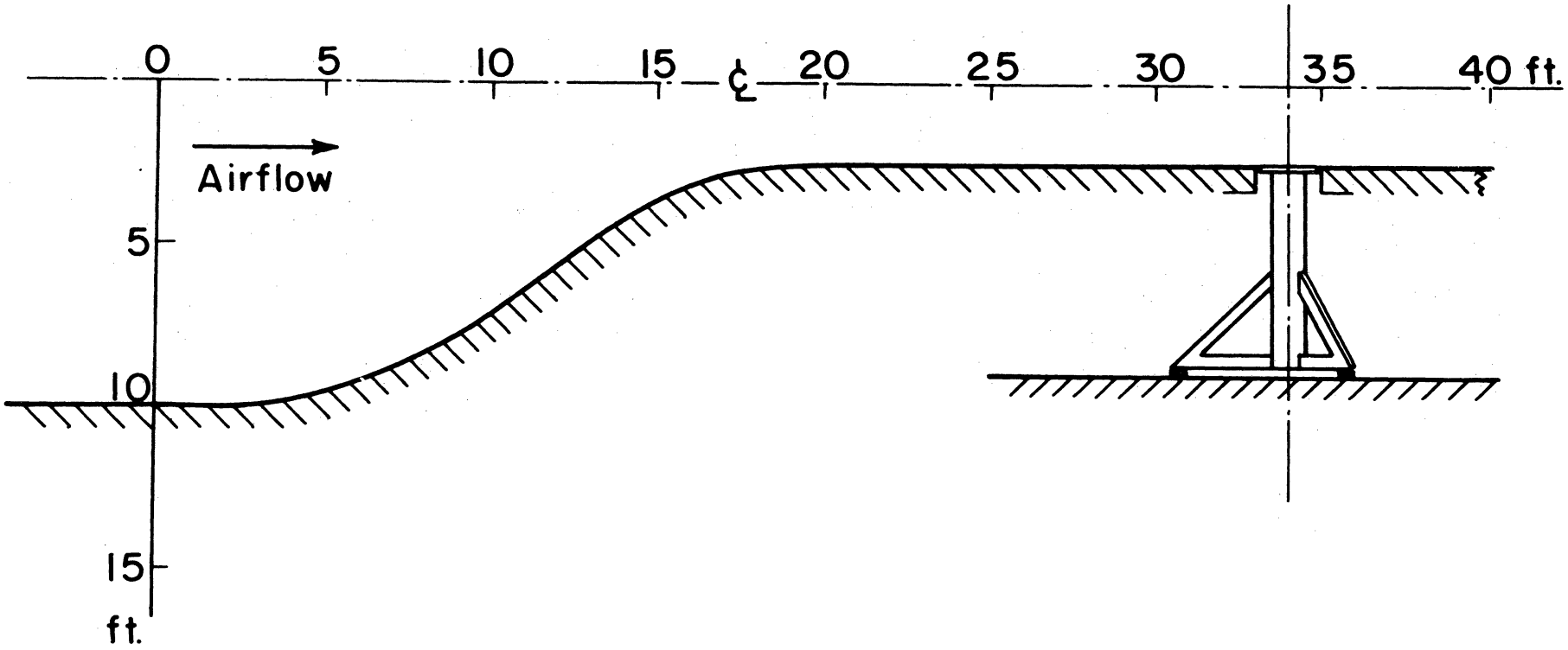

Fig. 1. Scale drawing of wind tunnel test section and massive vibration isolation mounting for the transducers.

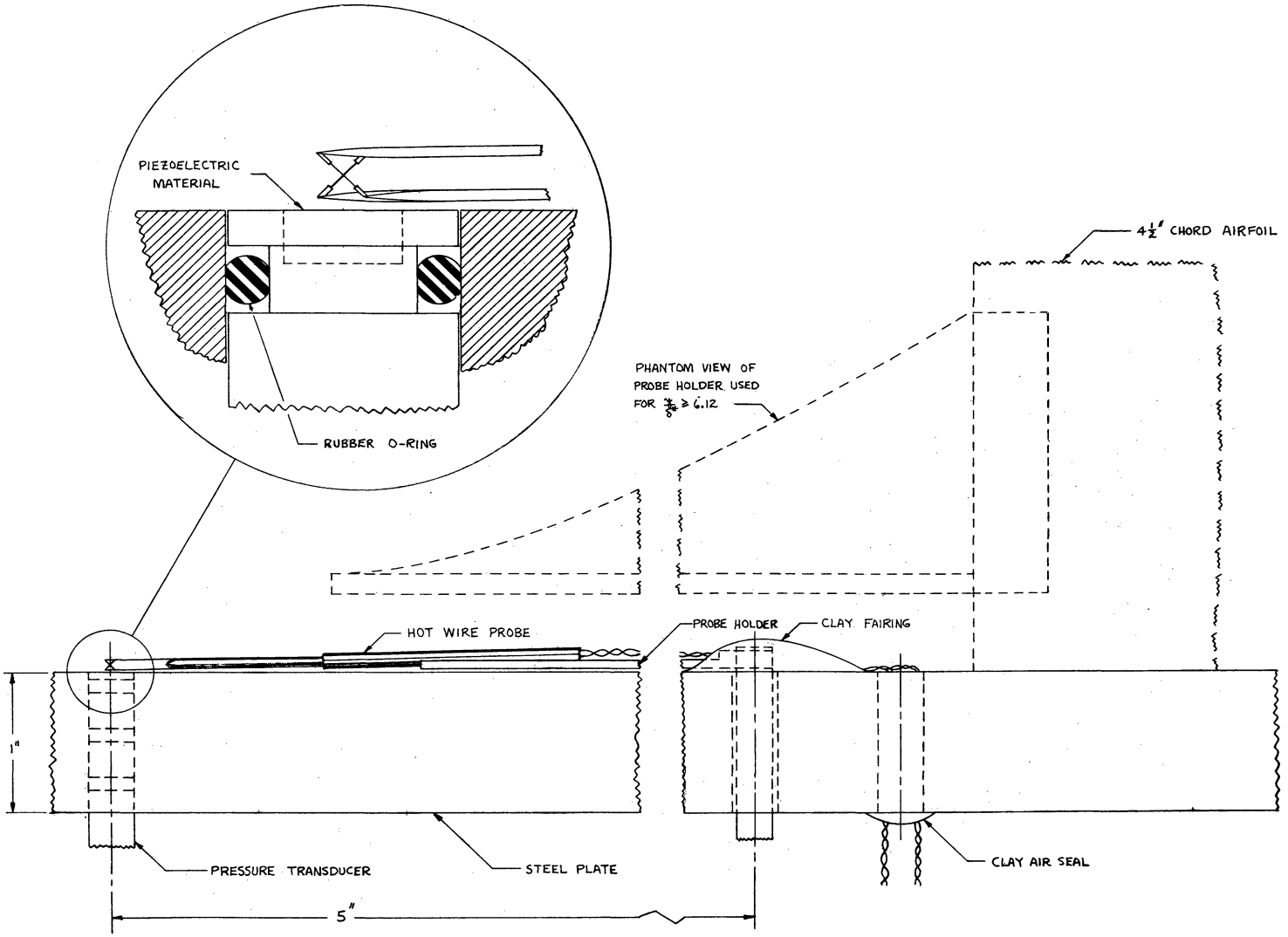

Fig. 2. Pressure transducer and hot wire installation. Hot wire shown at closest spacing to plate, 0.050 inch.

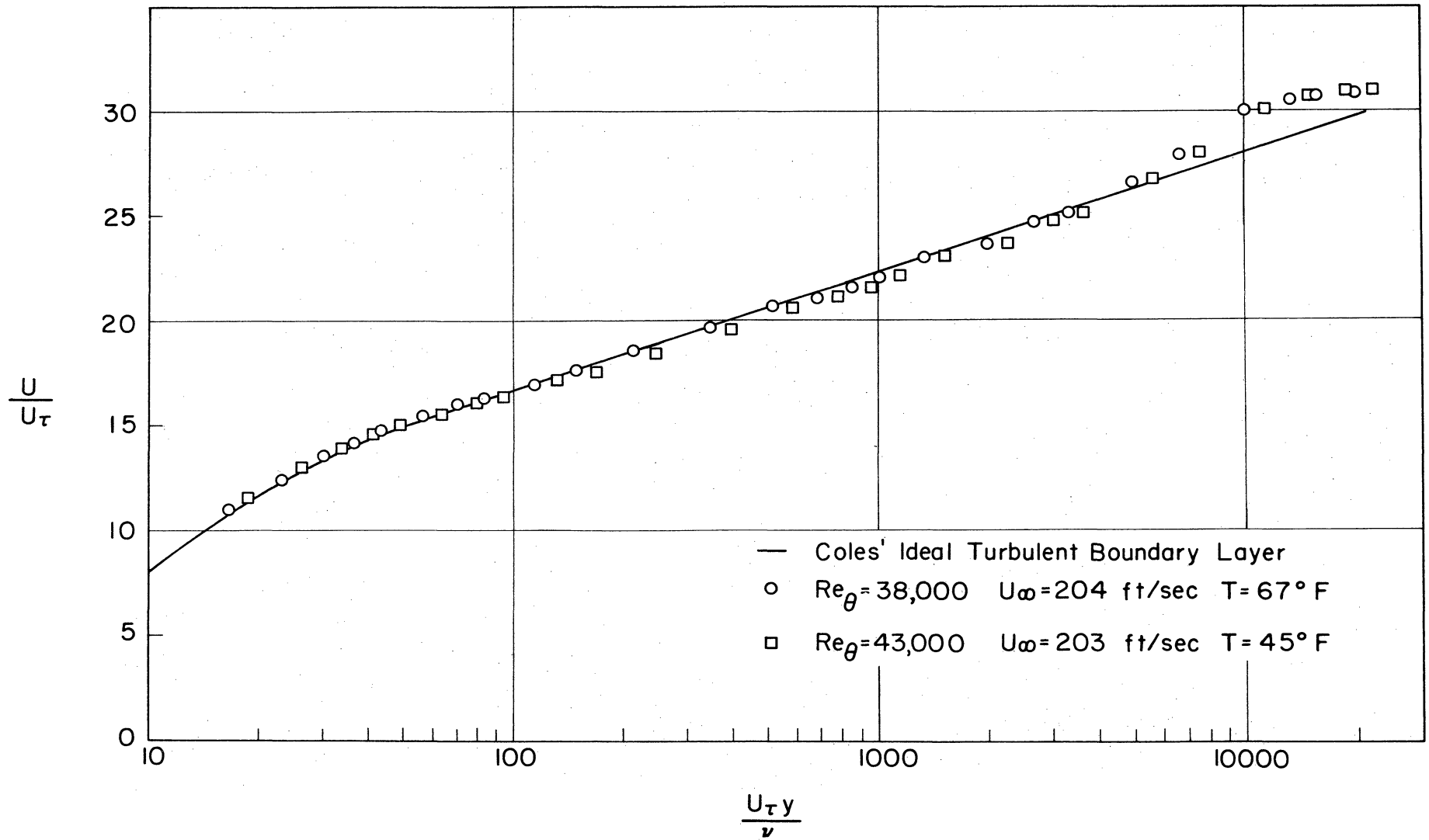

Fig. 3. Mean velocity profiles in the turbulent boundary layer. Refer to Table I for other boundary layer parameters.

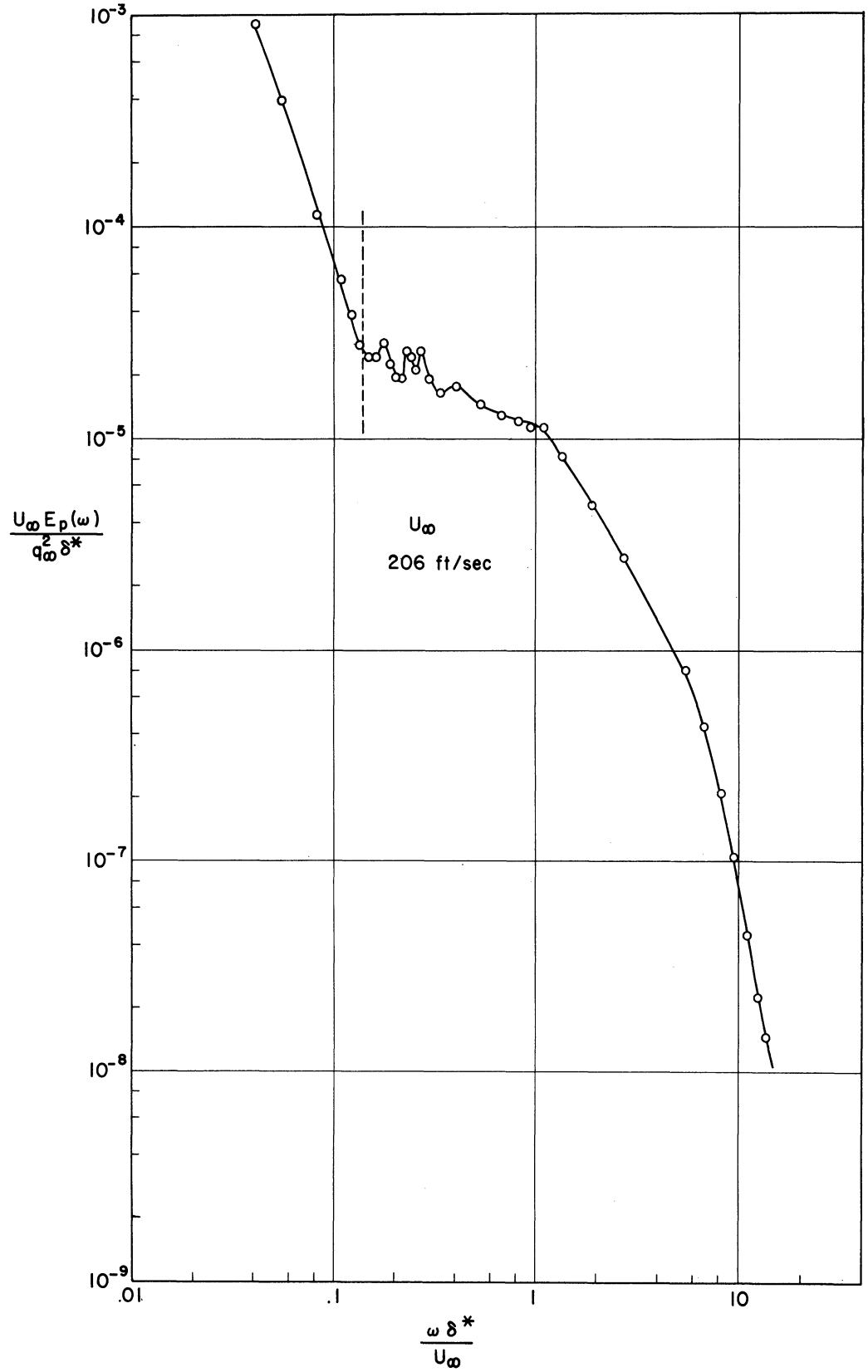

Fig. 4. Dimensionless power spectrum of the wall pressure. Vertical dashed line shows the frequency below which signals were rejected in the subsequent measurements.

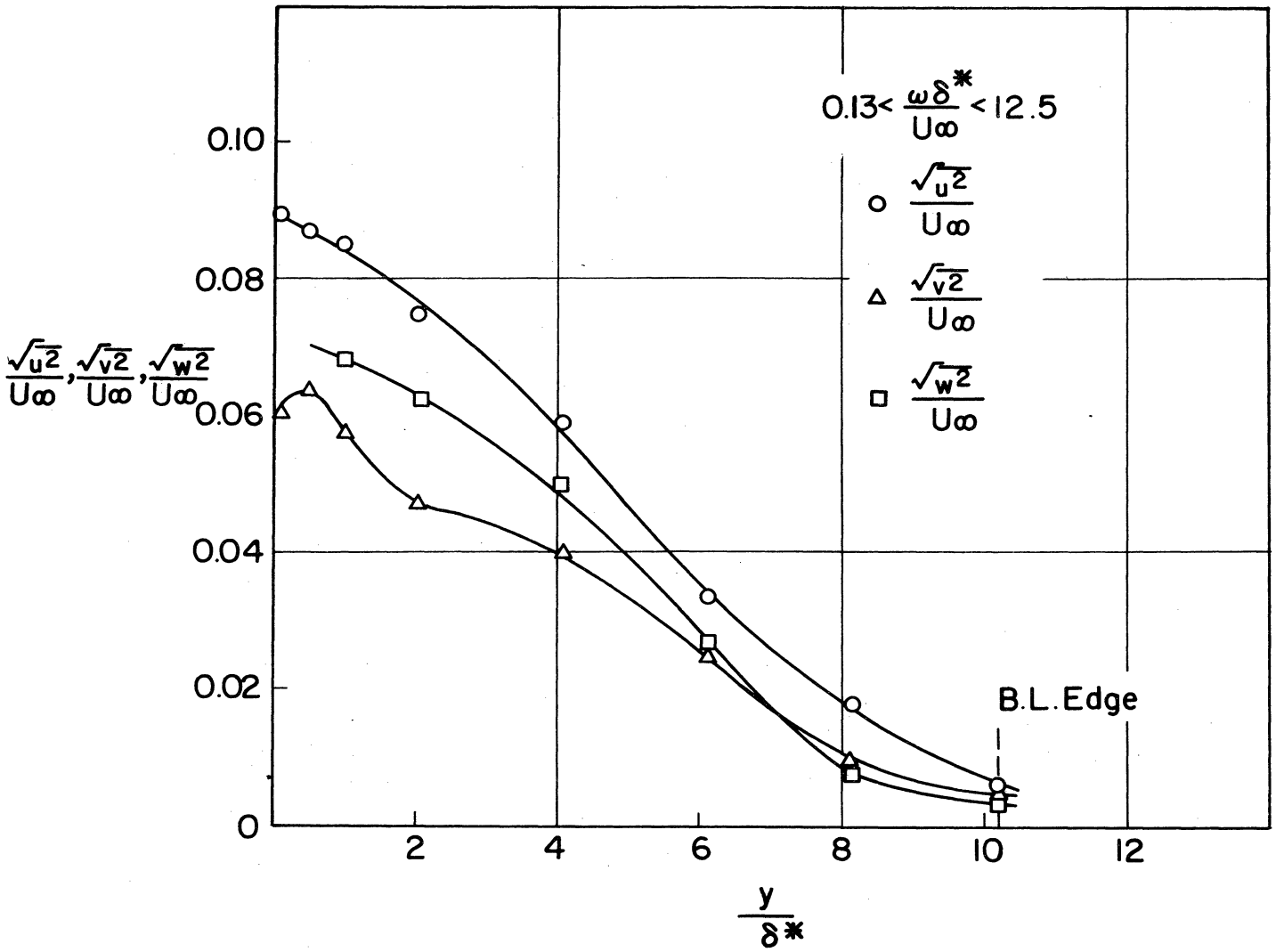

Fig. 5. Turbulent velocity intensity profiles in the frequency band used in the subsequent experiments.

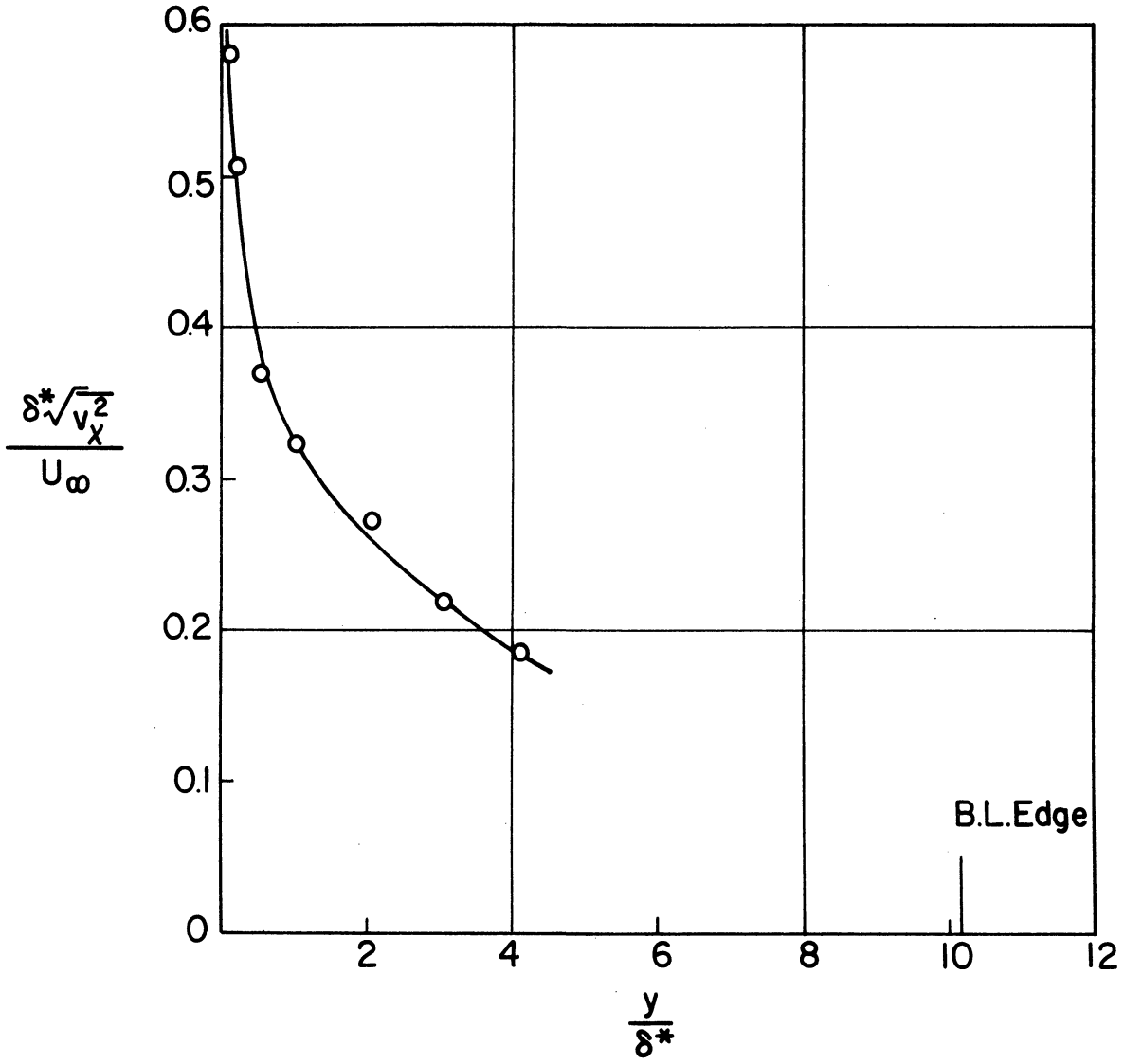

Fig. 6. Intensity profile of longitudinal derivative of velocity normal to wall.

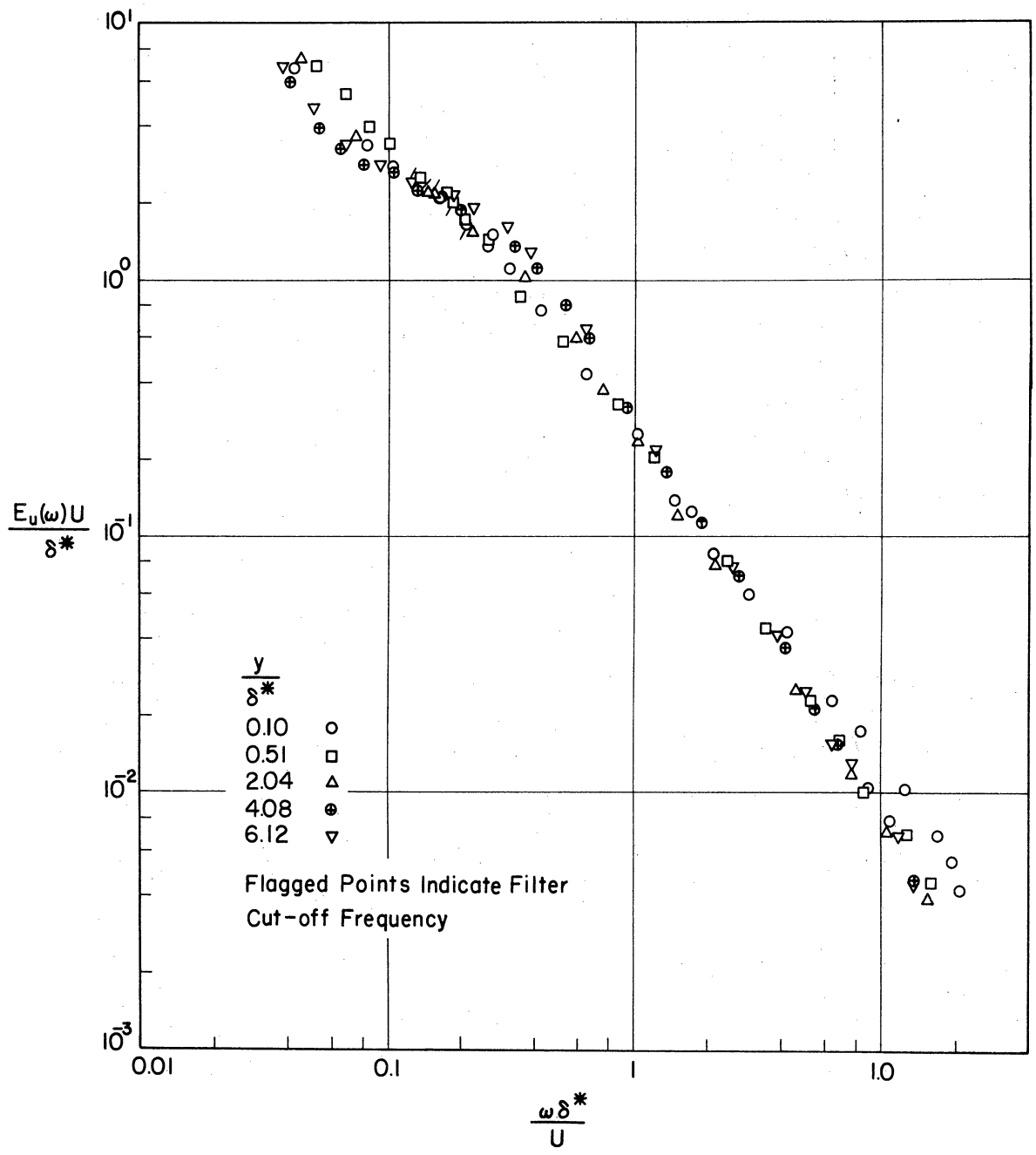

Fig. 7. Dimensionless normalized power spectra of the longitudinal velocity components at various heights in the boundary layer. Spectra are normalized to have unit area in the frequency band of the subsequent experiments.

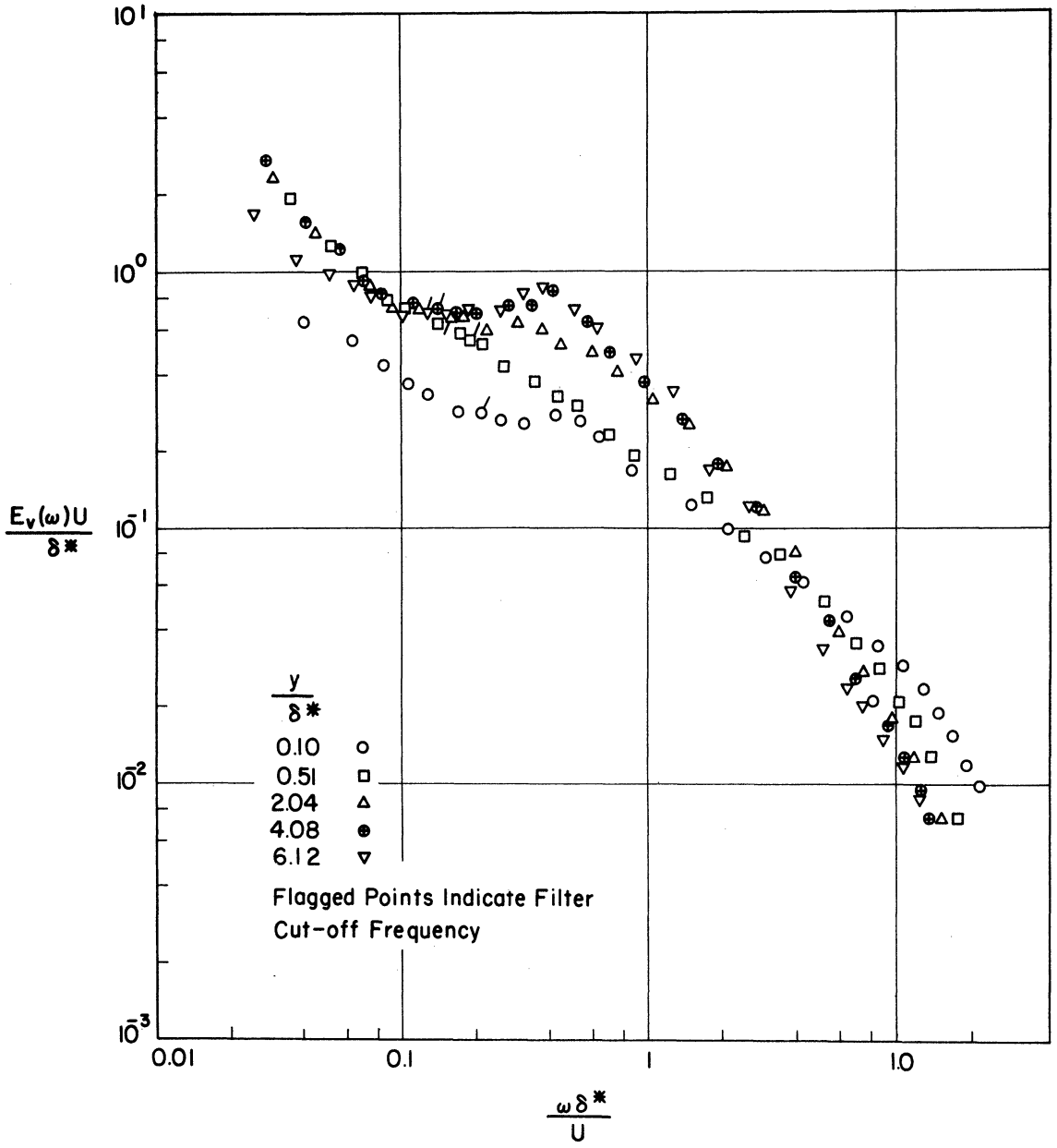

Fig. 8. Dimensionless normalized power spectra of the velocity components normal to the wall at various heights in the boundary layer. Spectra are normalized to have unit area in the frequency band of the subsequent experiments.

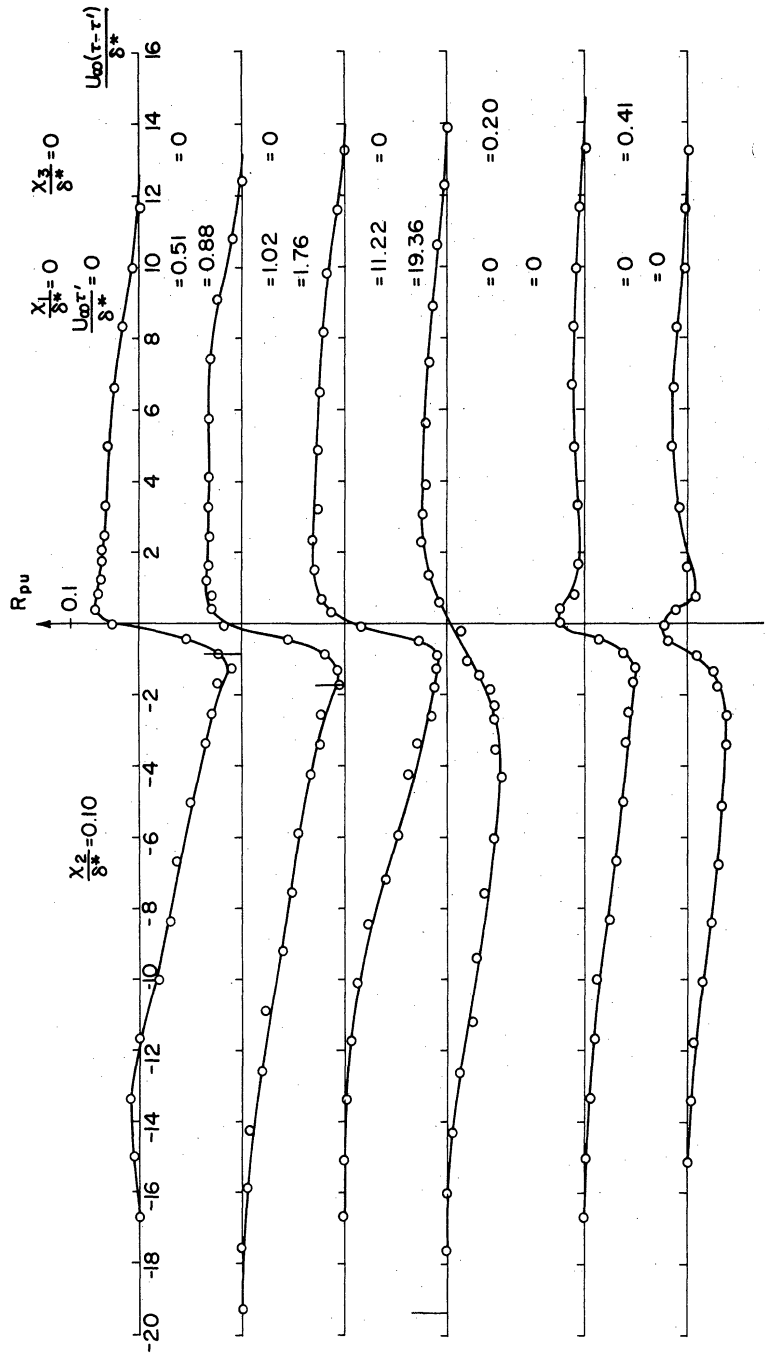

Fig. 9. Measured values of the space-time correlation of fluctuating velocity with fluctuating wall pressure.

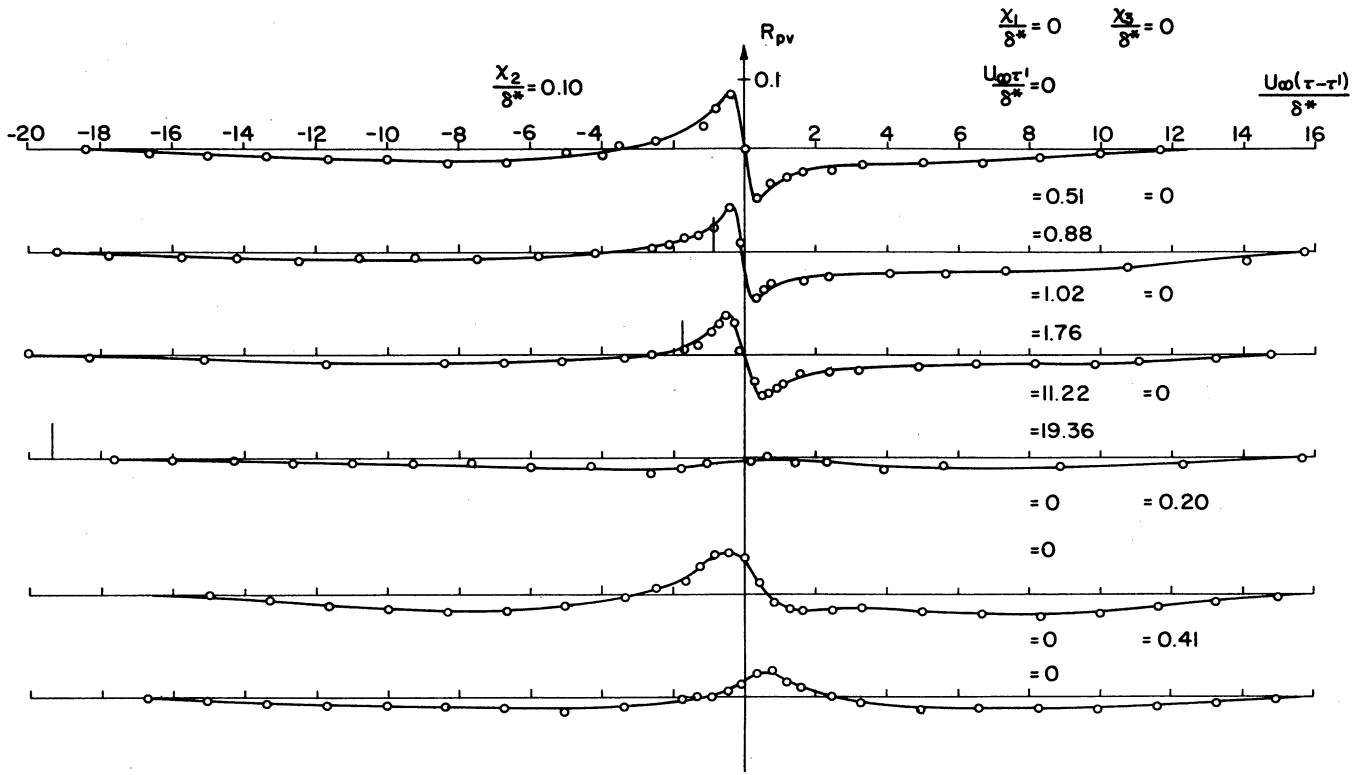

Fig. 10. Measured values of the space-time correlation of fluctuating velocity with fluctuating wall pressure.

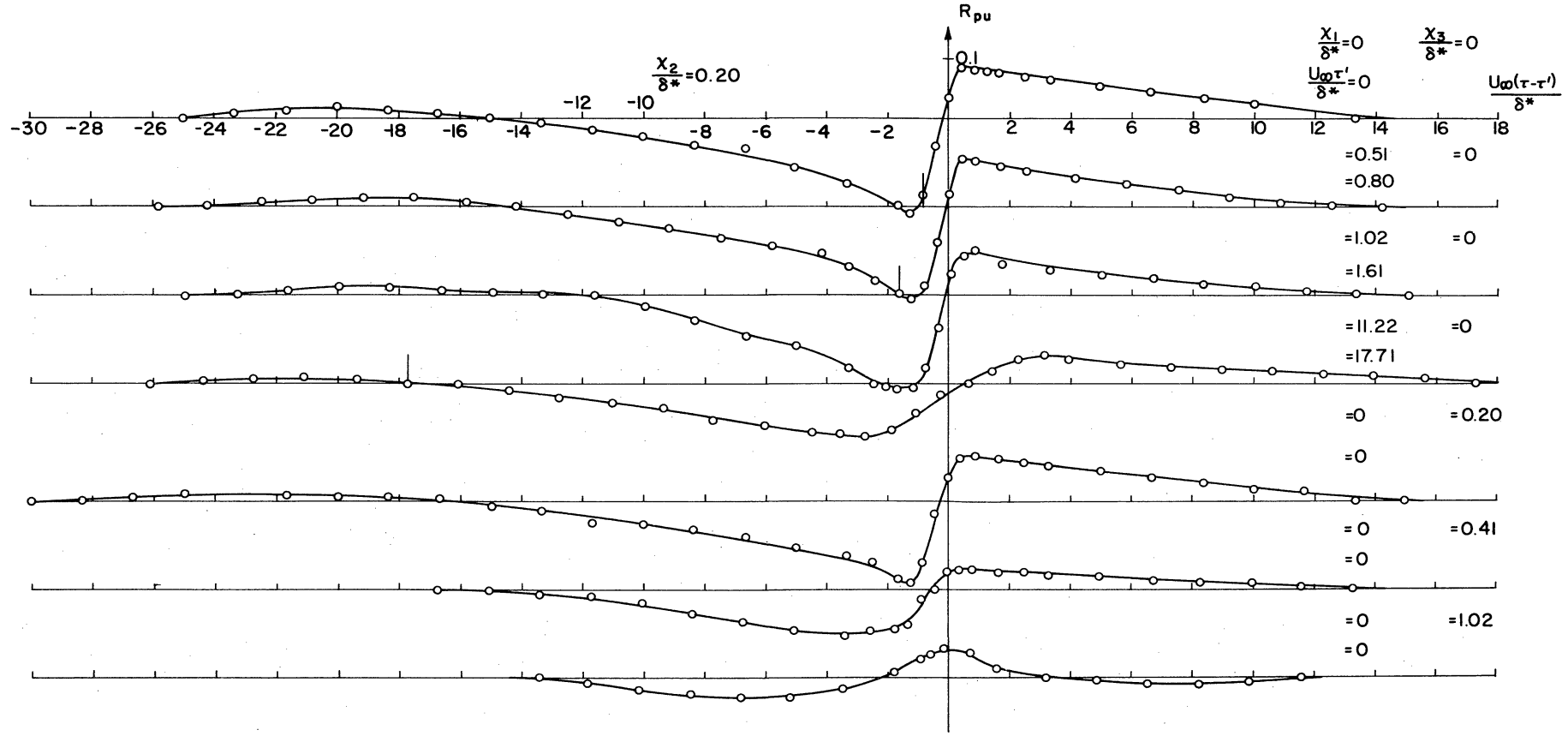

Fig. 11. Measured values of the space-time correlation of fluctuating velocity with fluctuating wall pressure.

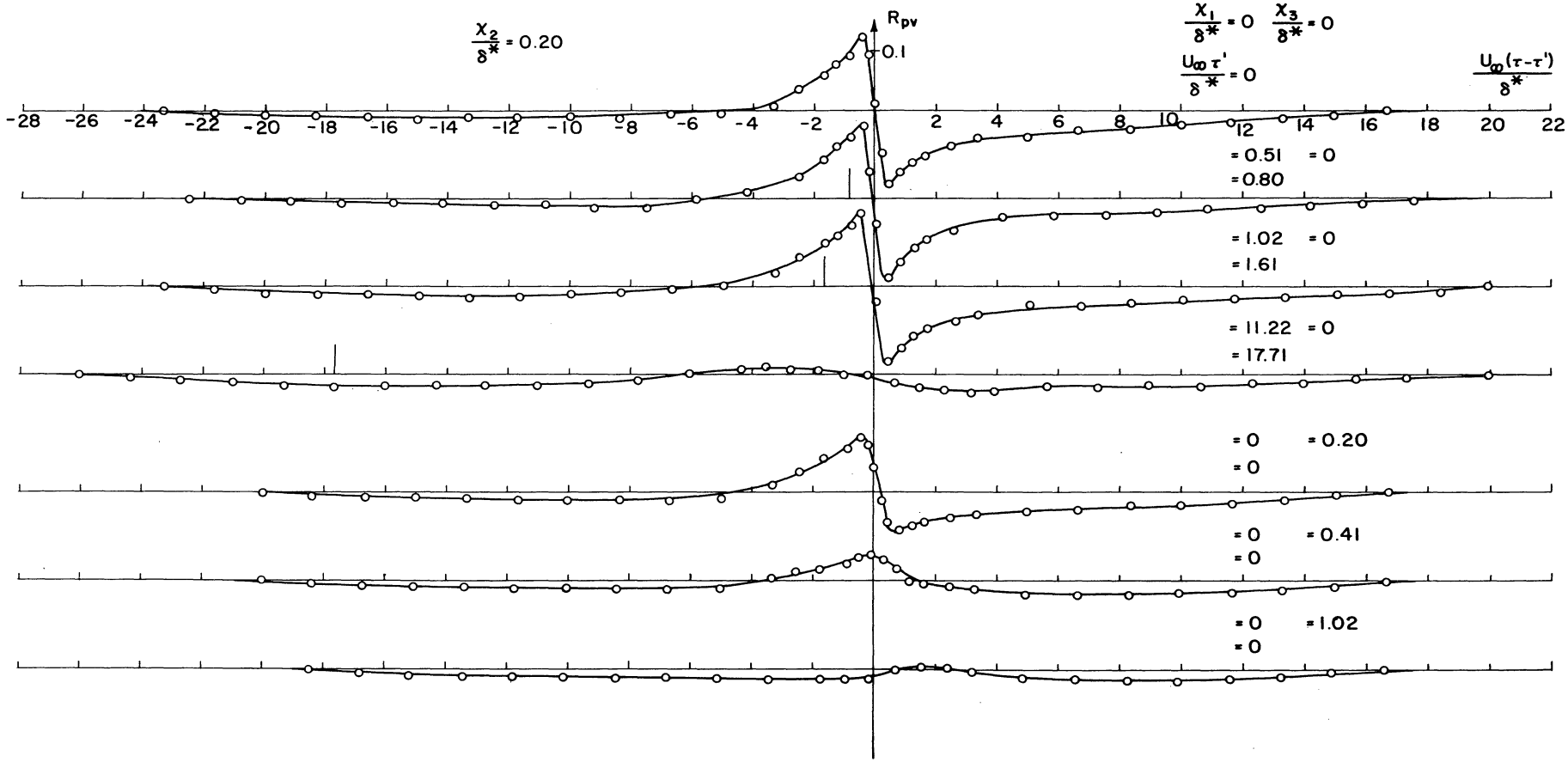

Fig. 12. Measured values of the space-time correlation of fluctuating velocity with fluctuating wall pressure.

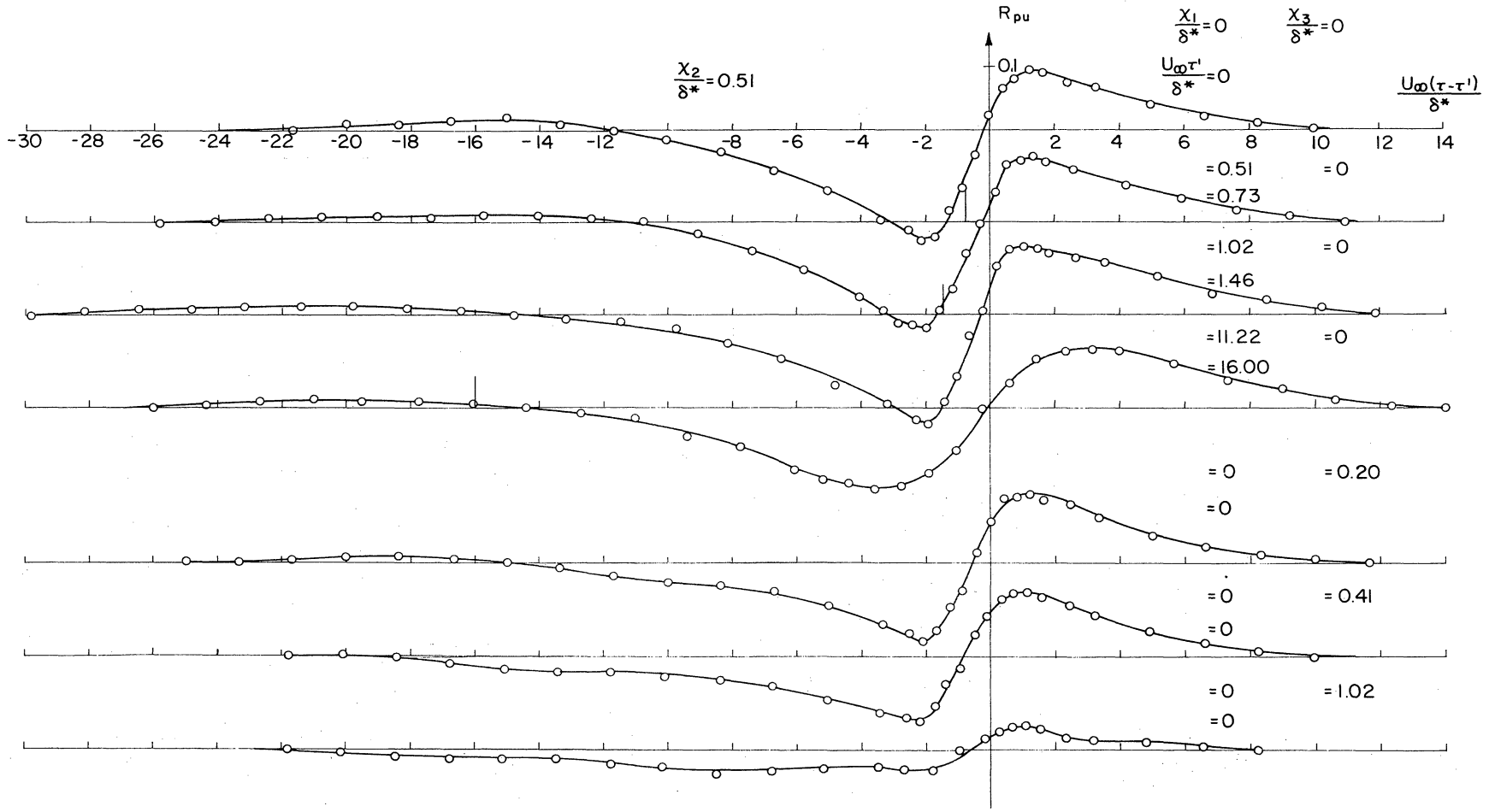

Fig. 13. Measured values of the space-time correlation of fluctuating velocity with fluctuating wall pressure.

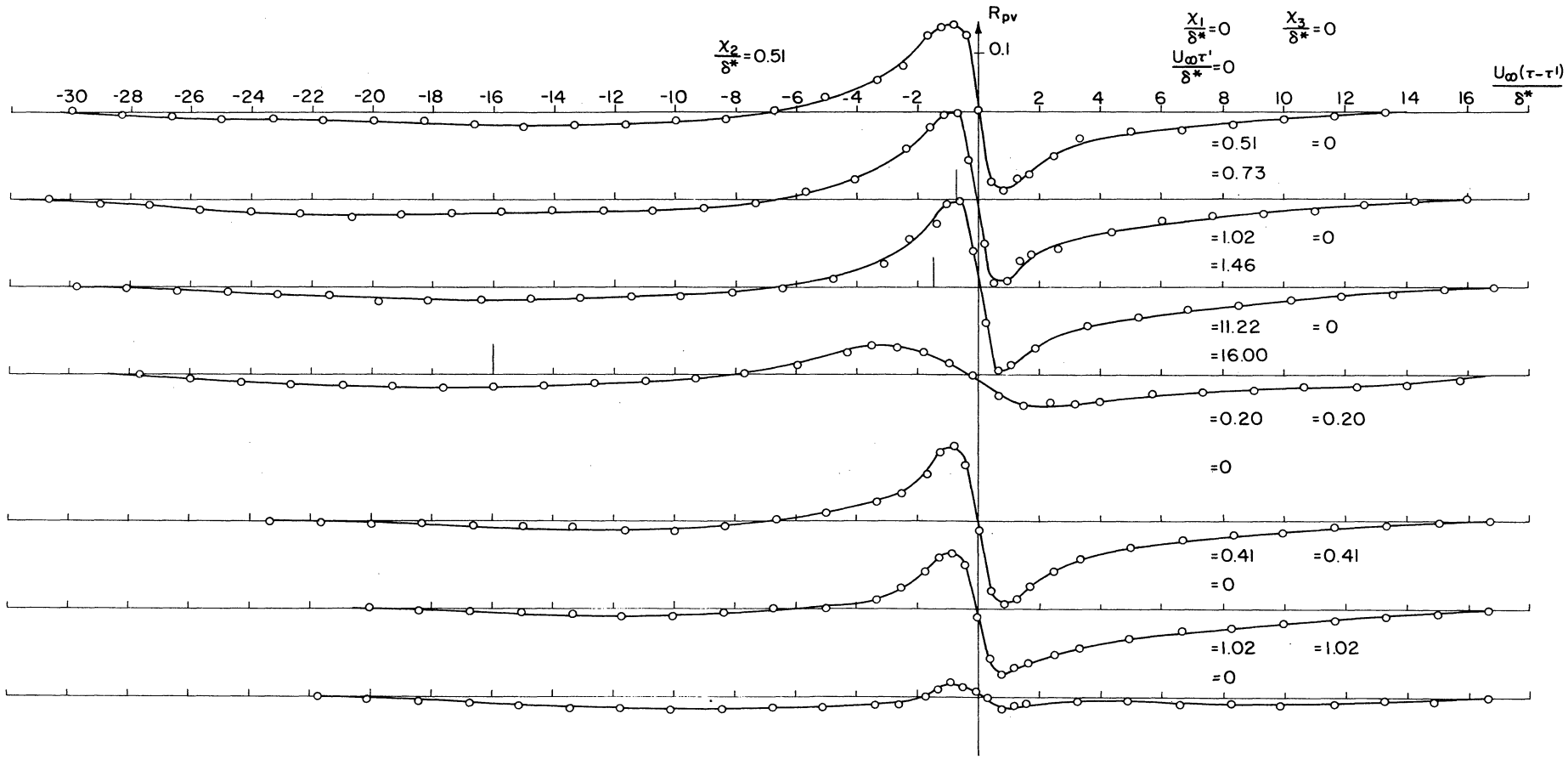

Fig. 14. Measured values of the space-time correlation of fluctuating velocity with fluctuating wall pressure.

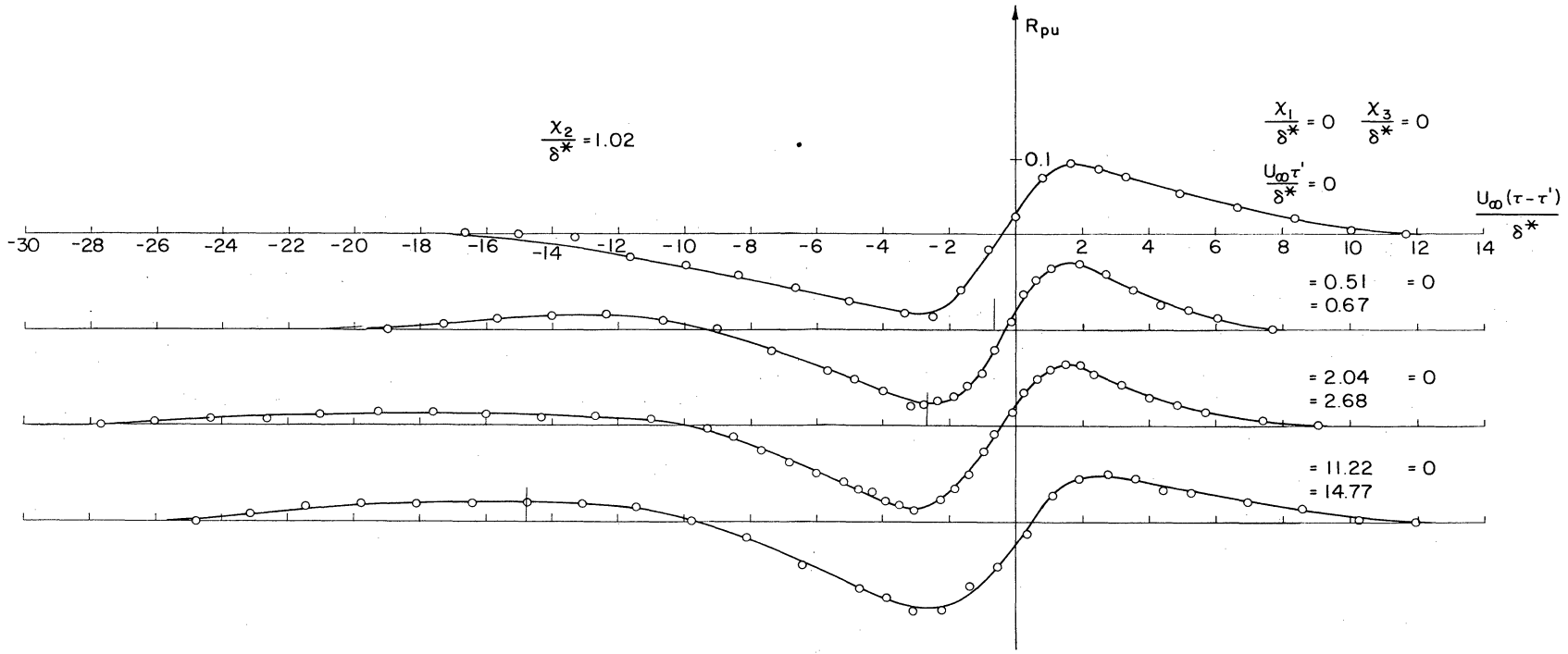

Fig. 15. Measured values of the space-time correlation of fluctuating velocity with fluctuating wall pressure.

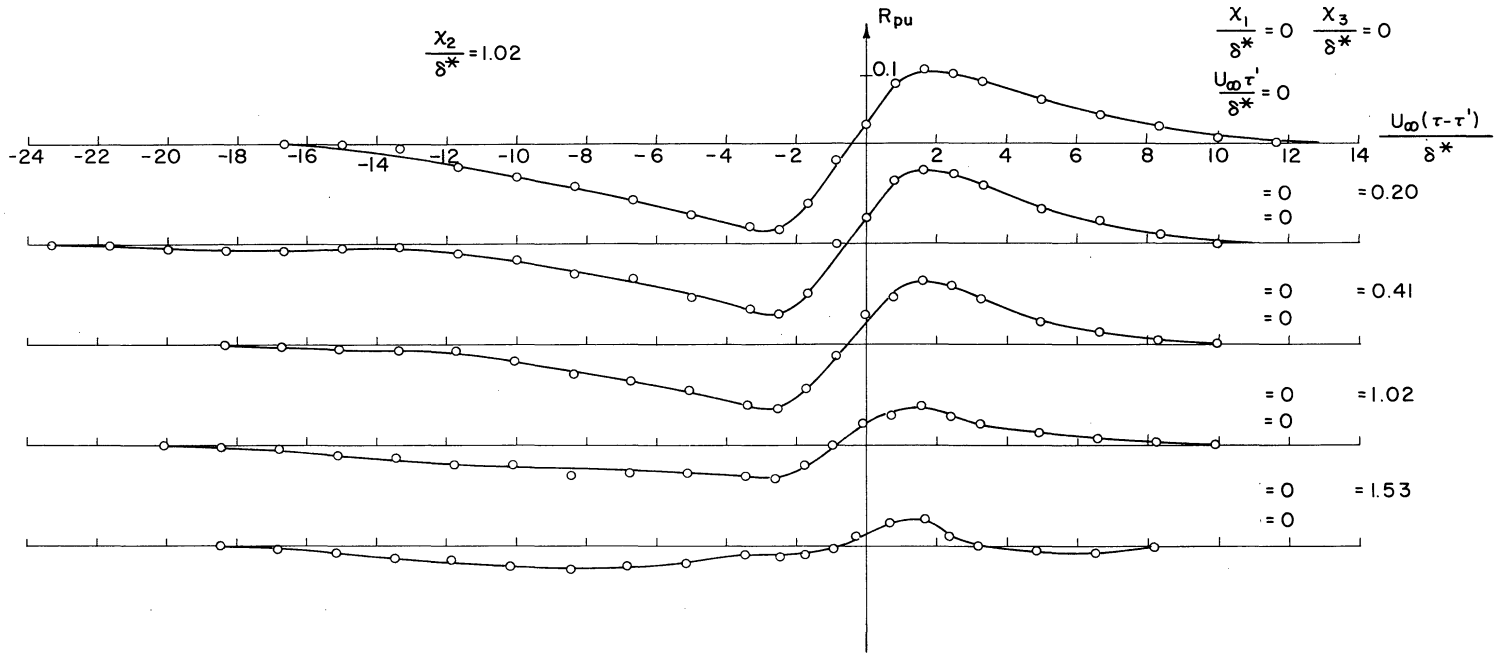

Fig. 16. Measured values of the space-time correlation of fluctuating velocity with fluctuating wall pressure.

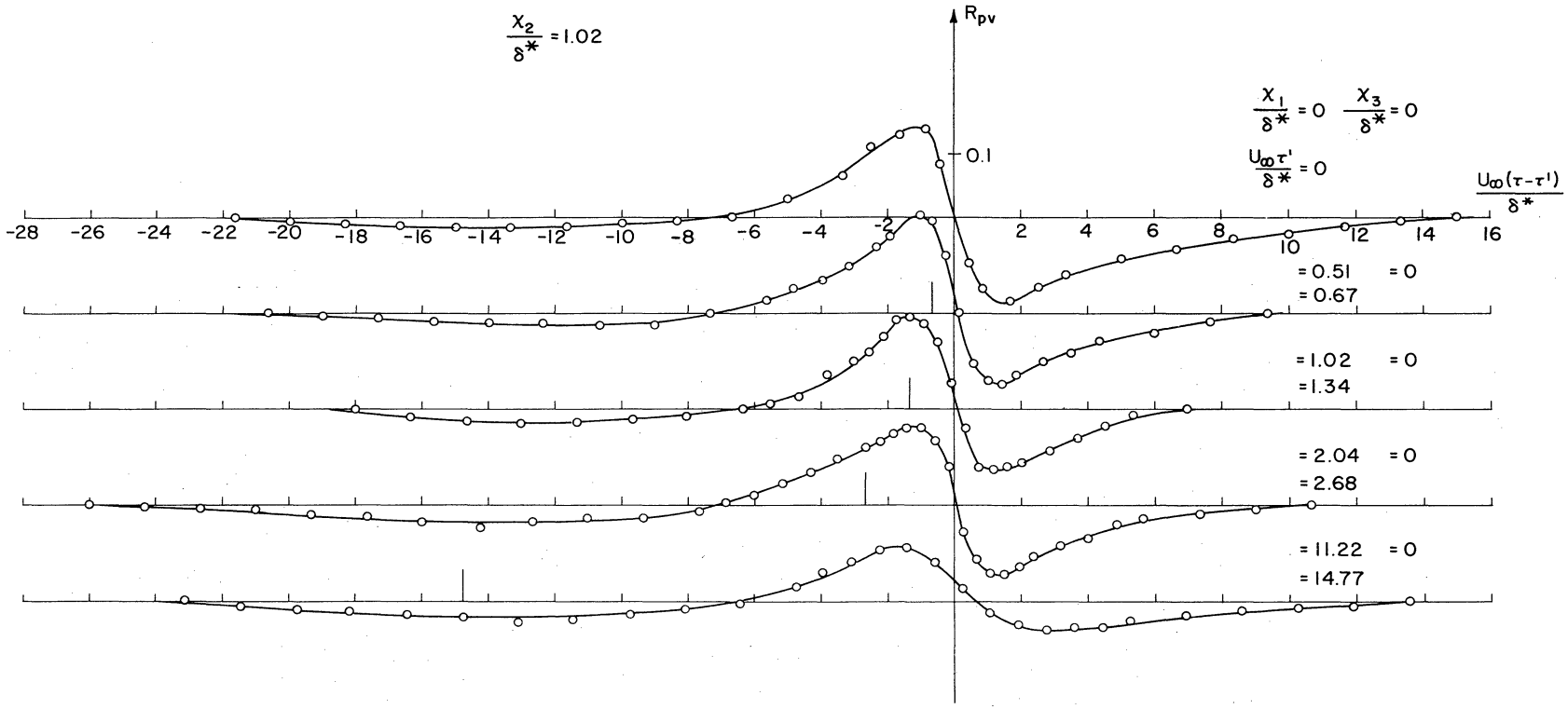

Fig. 17. Measured values of the space-time correlation of fluctuating velocity with fluctuating wall pressure.

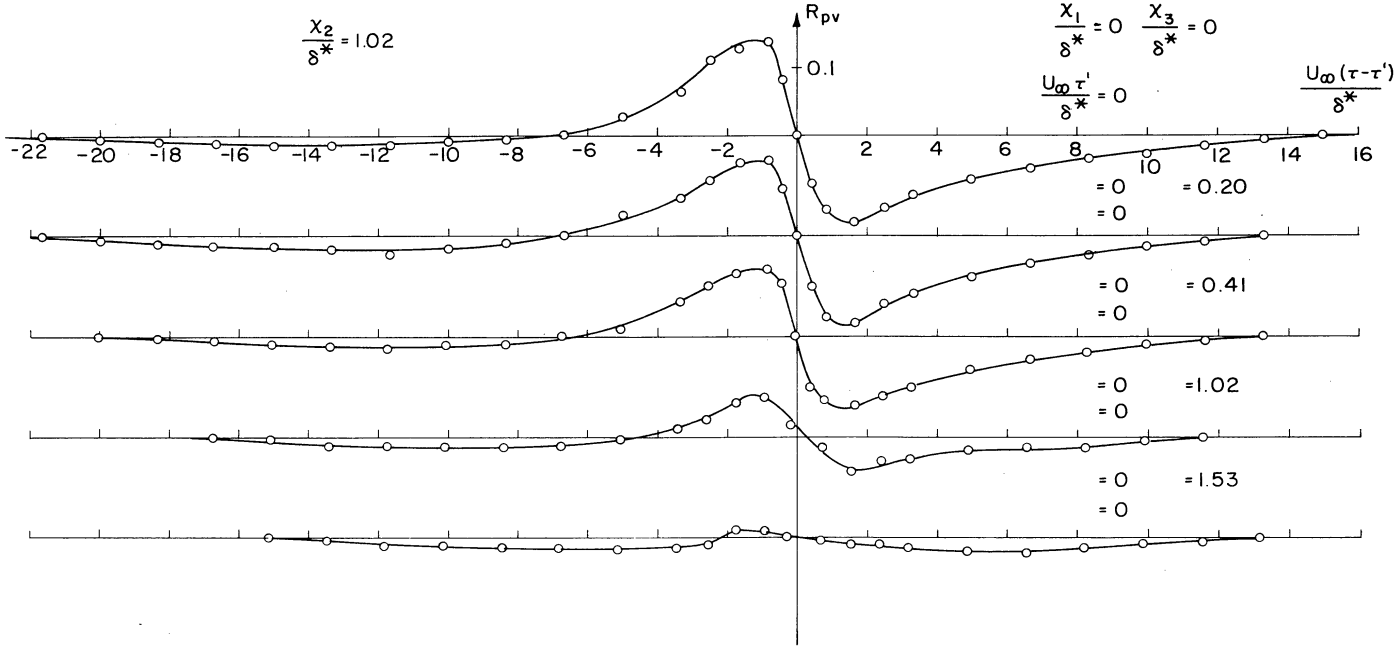

Fig. 18. Measured values of the space-time correlation of fluctuating velocity with fluctuating wall pressure.

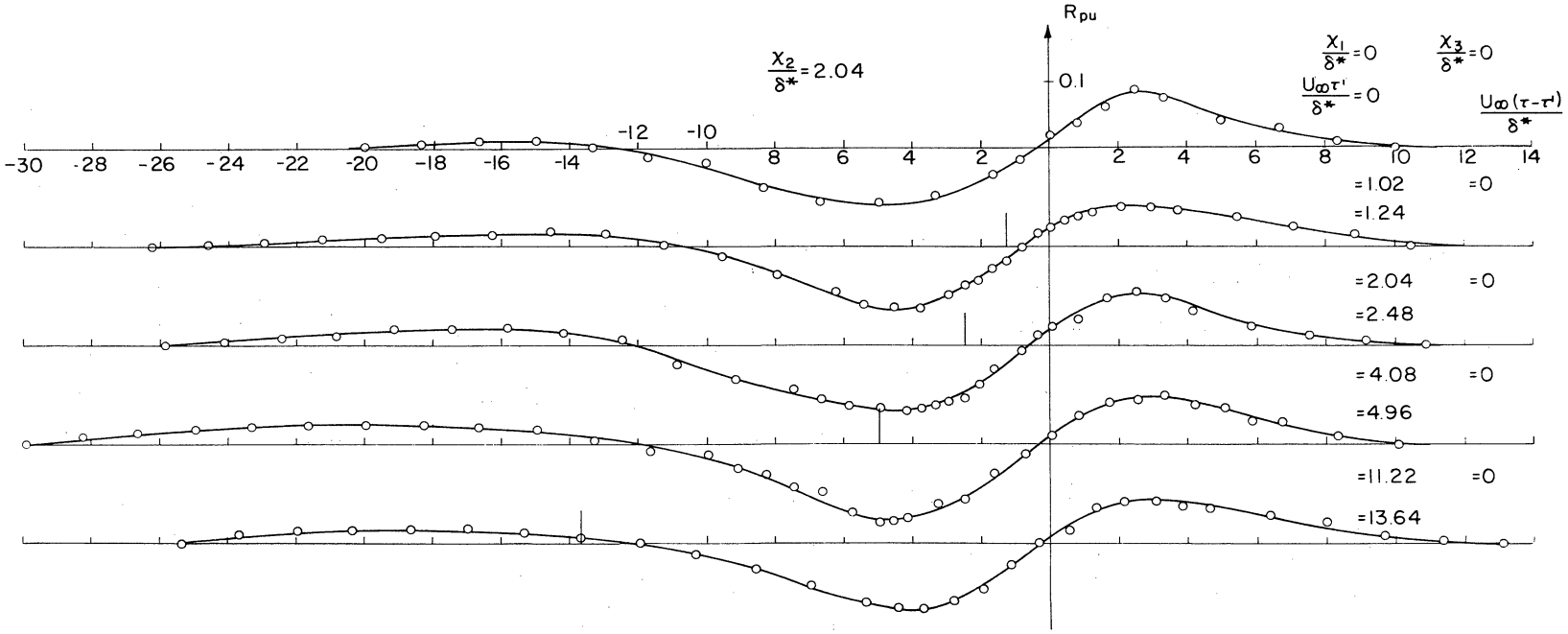

Fig. 19. Measured values of the space-time correlation of fluctuating velocity with fluctuating wall pressure.

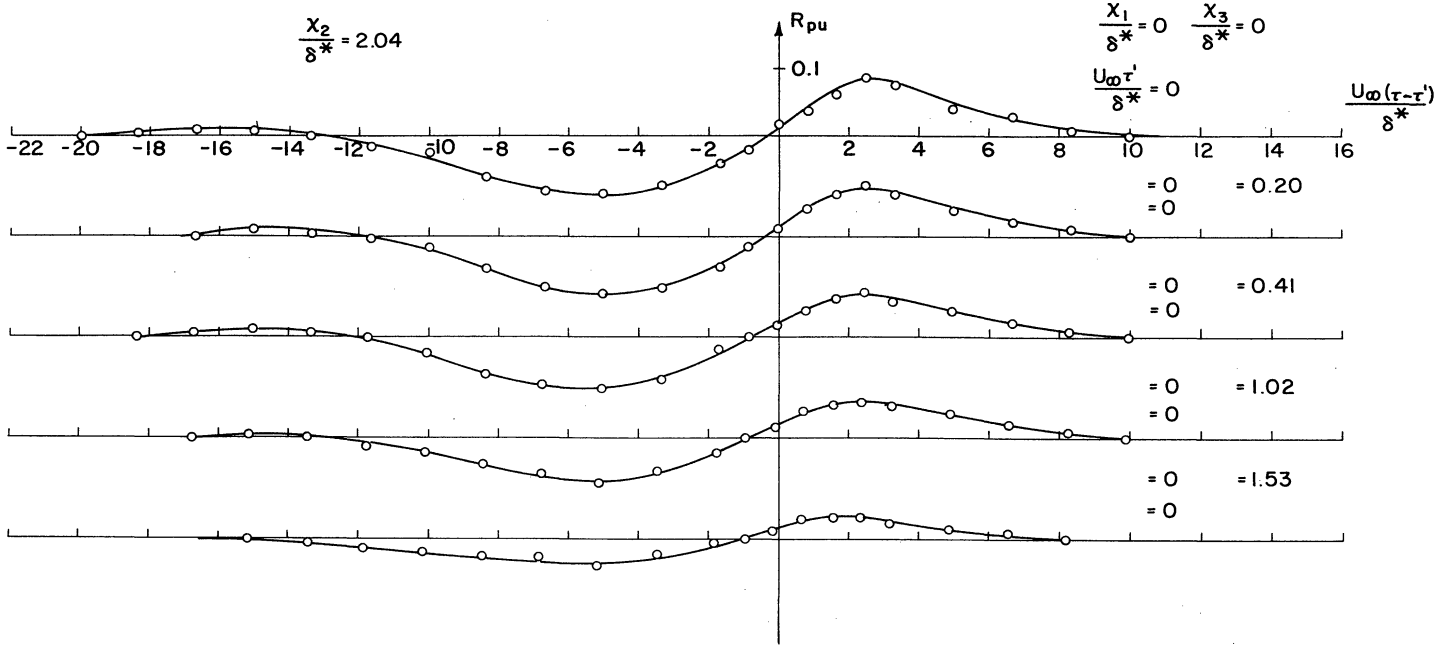

Fig. 20. Measured values of the space-time correlation of fluctuating velocity with fluctuating wall pressure.

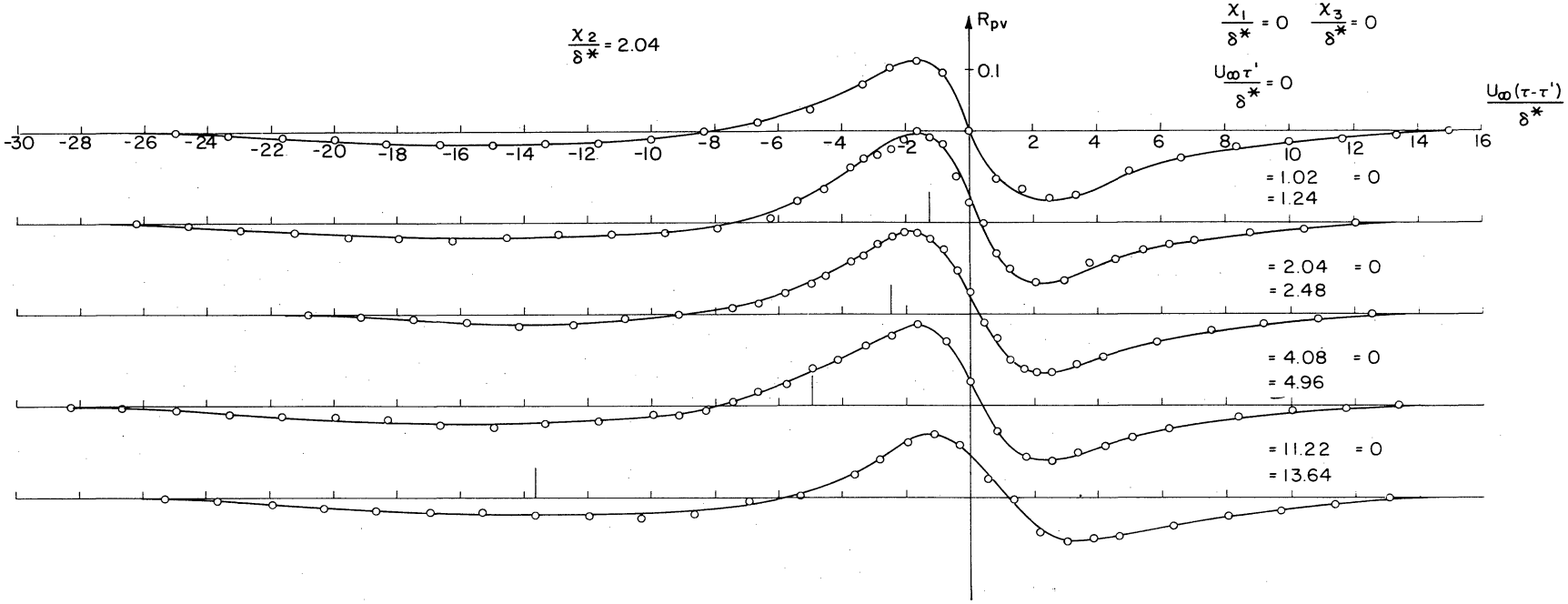

Fig. 21. Measured values of the space-time correlation of fluctuating velocity with fluctuating wall pressure.

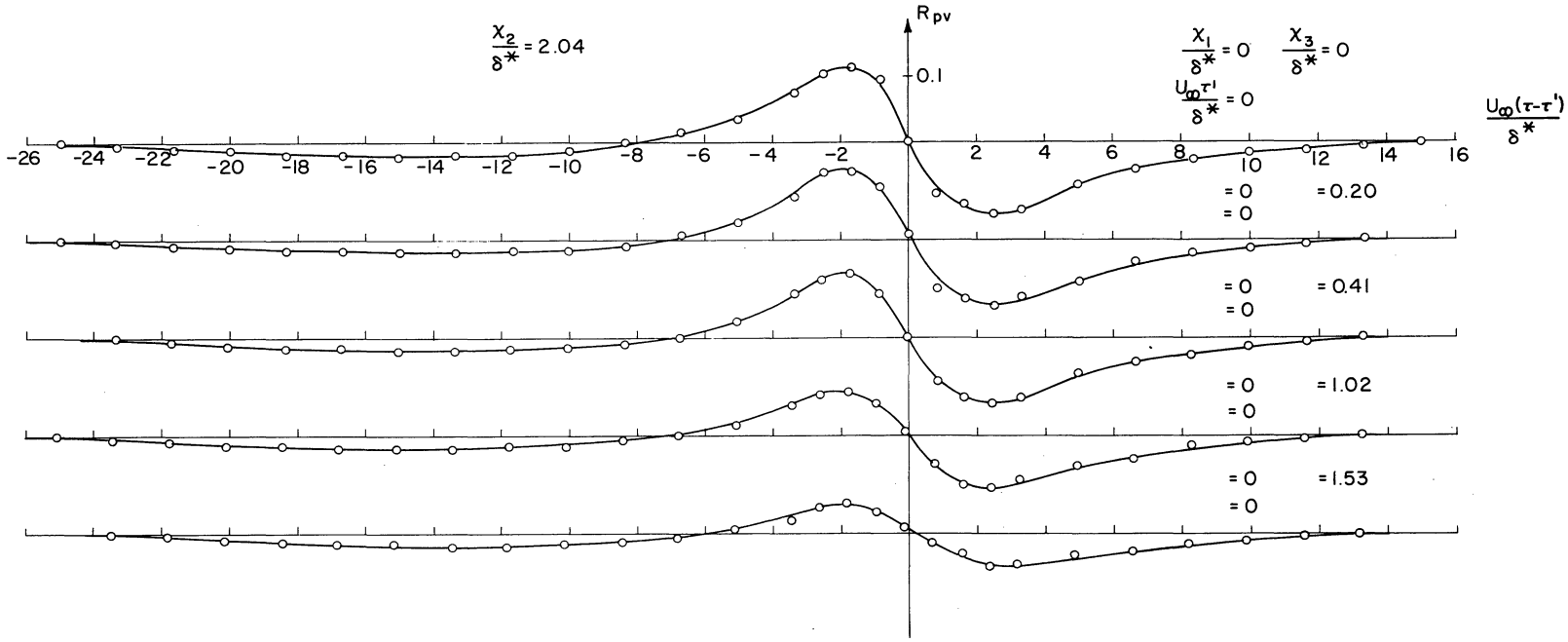

Fig. 22. Measured values of the space-time correlation of fluctuating velocity with fluctuating wall pressure.

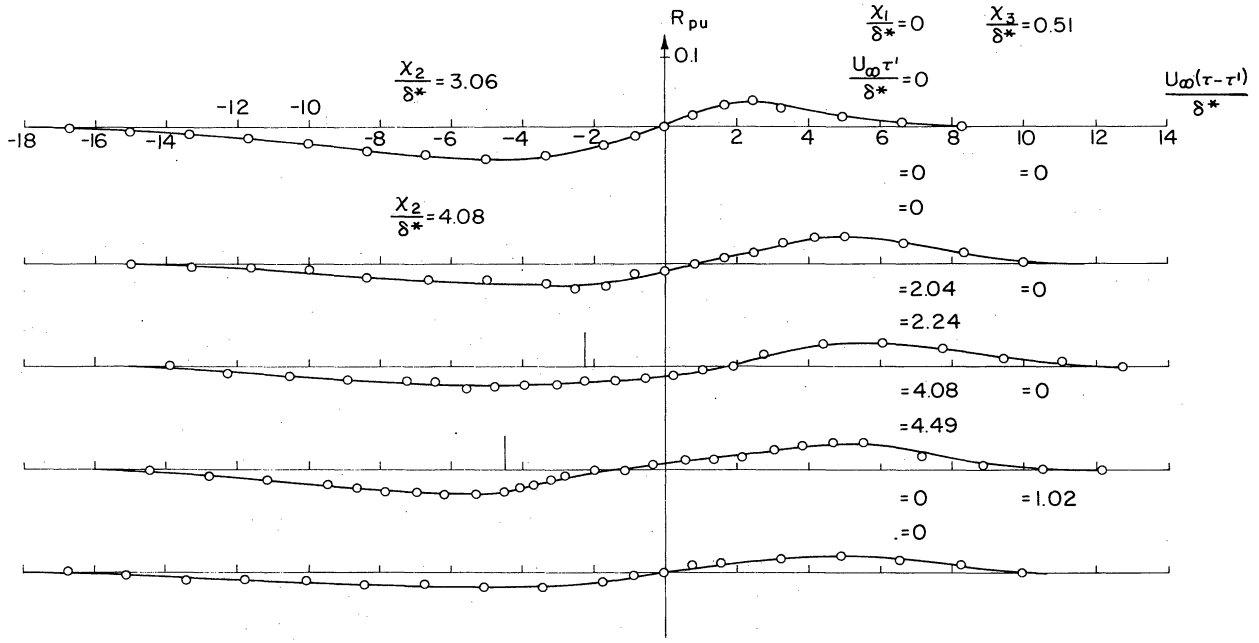

Fig. 23. Measured values of the space-time correlation of fluctuating velocity with fluctuating wall pressure.

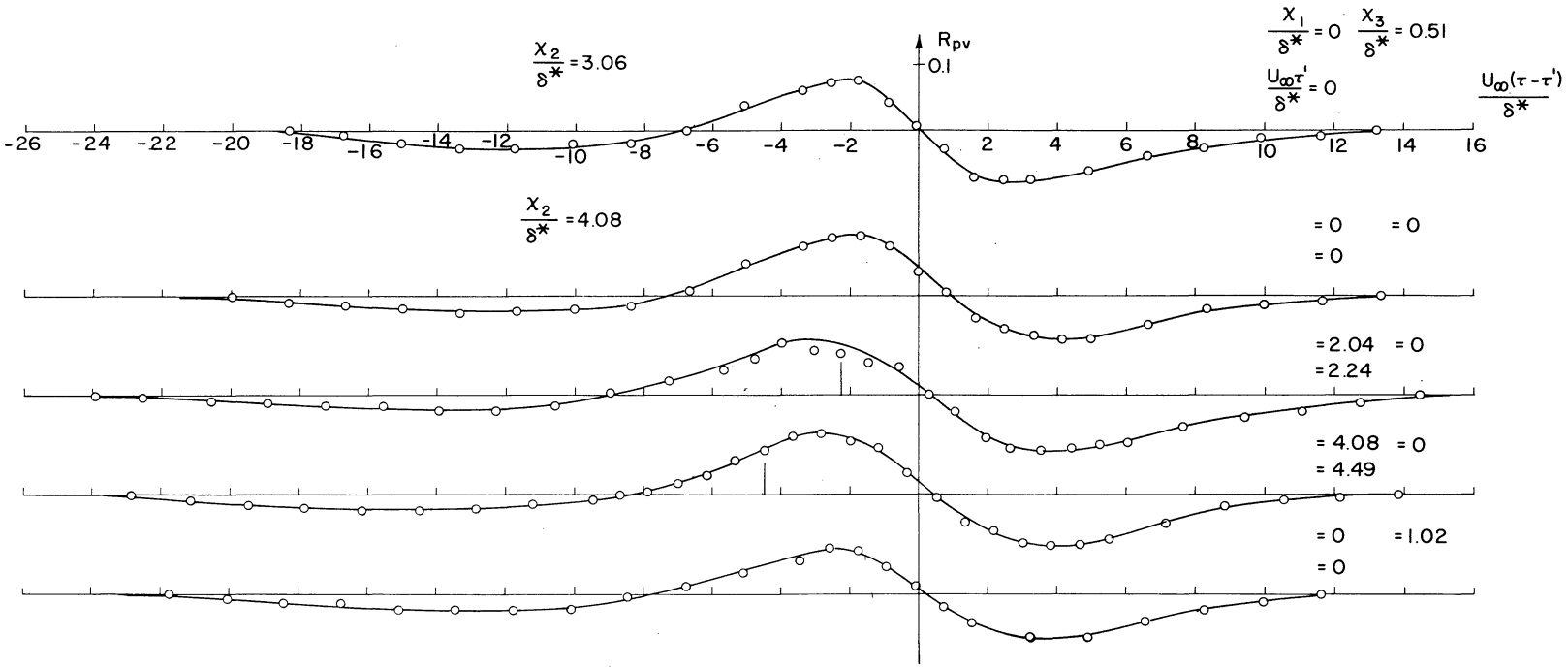

Fig. 24. Measured values of the space-time correlation of fluctuating velocity with fluctuating wall pressure.

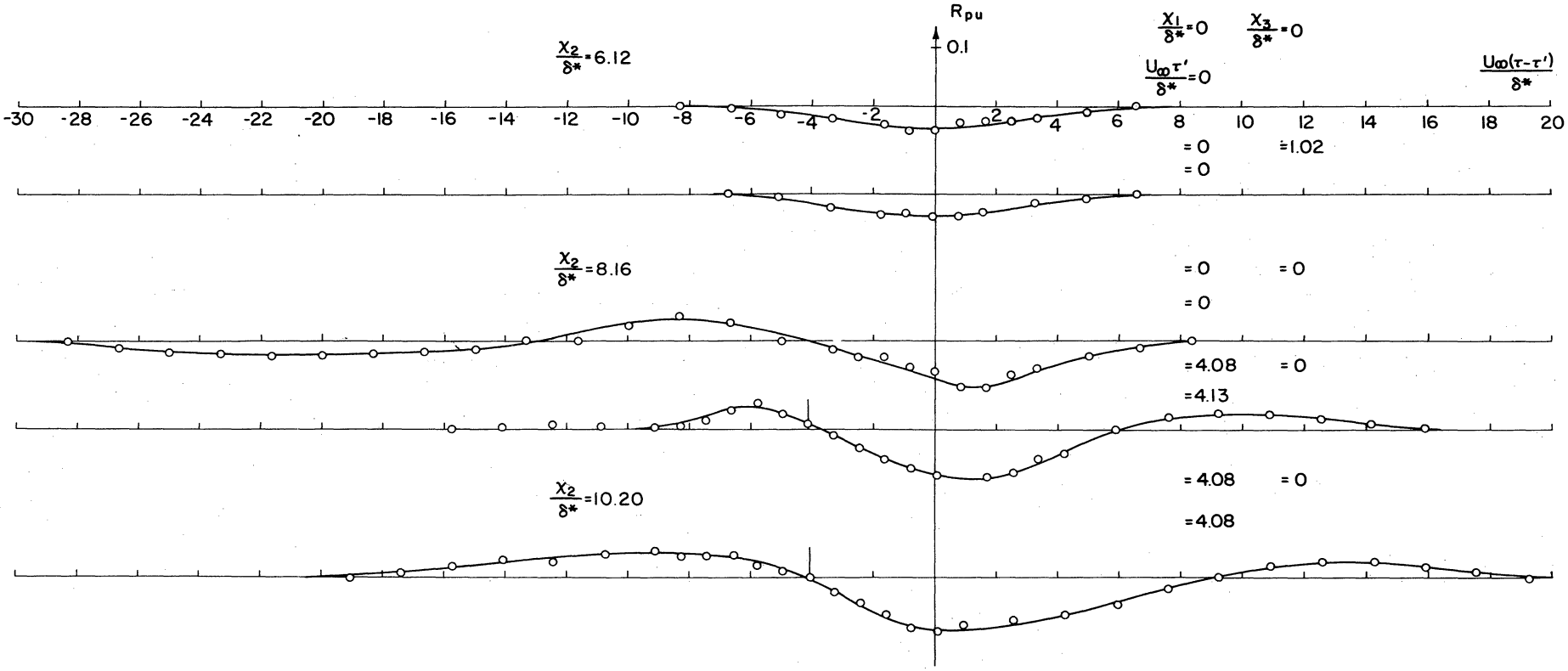

Fig. 25. Measured values of the space-time correlation of fluctuating velocity with fluctuating wall pressure.

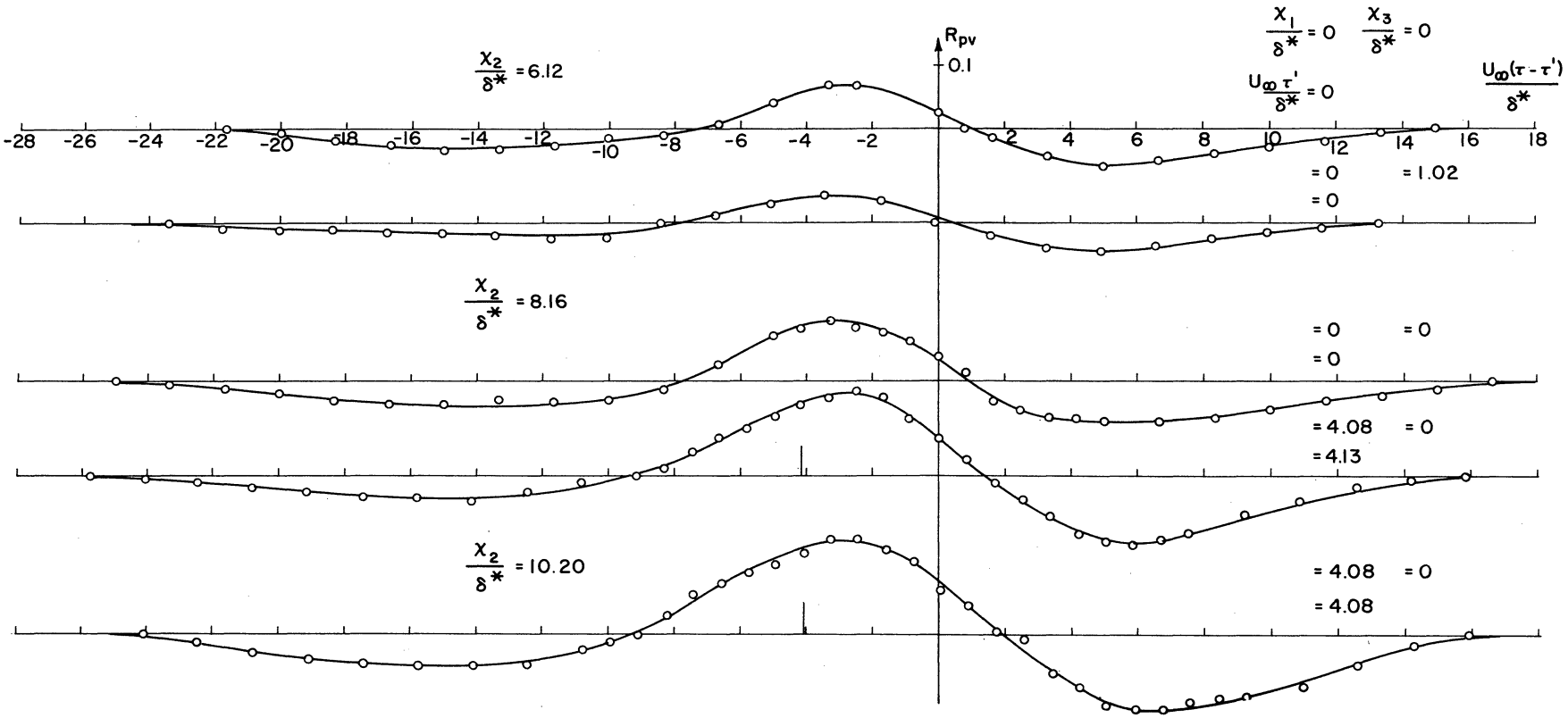

Fig. 26. Measured values of the space-time correlation of fluctuating velocity with fluctuating wall pressure.

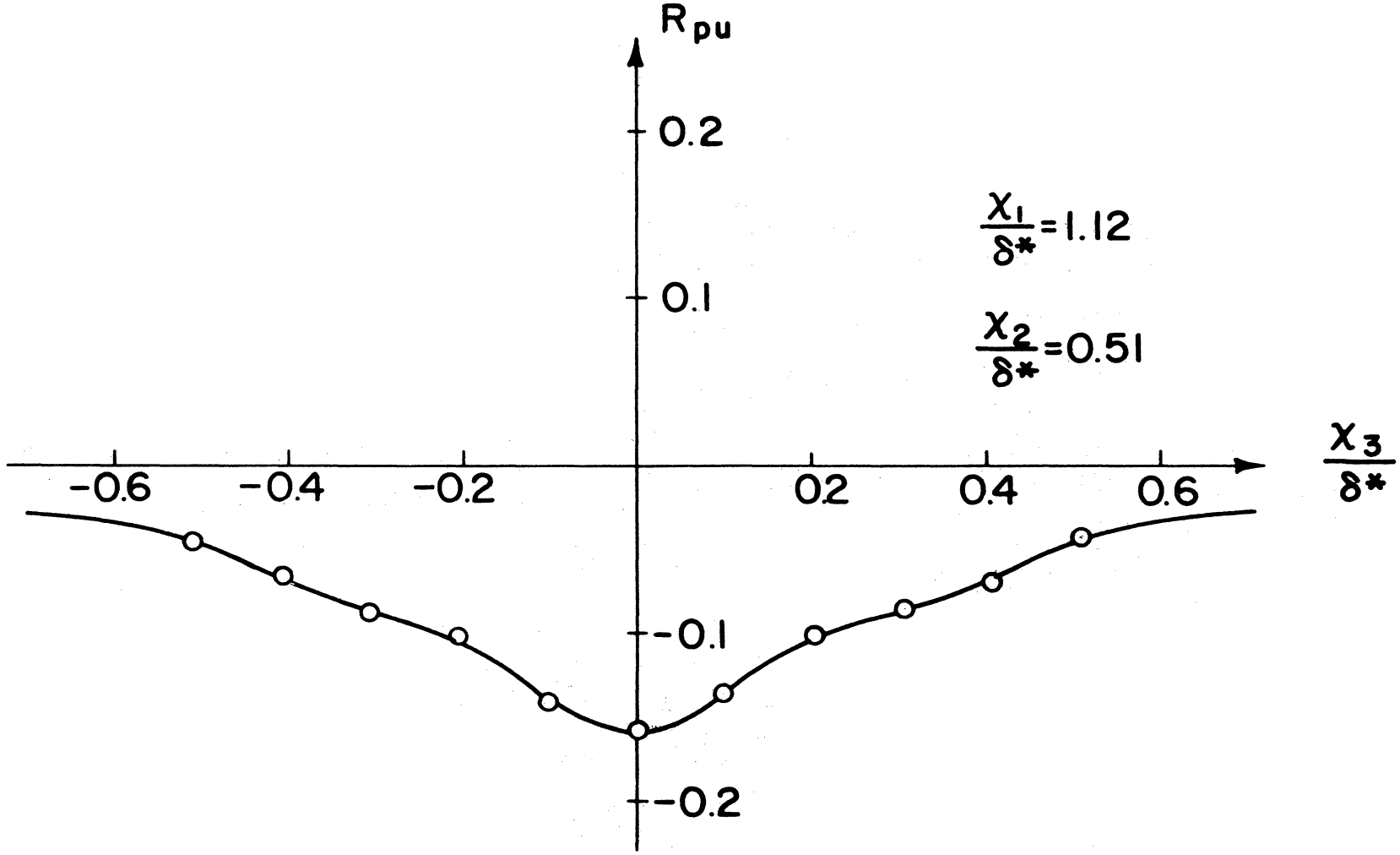

Fig. 27. Measured values of the spatial correlation of fluctuating longitudinal velocity with fluctuating wall pressure showing symmetry in the transverse direction.

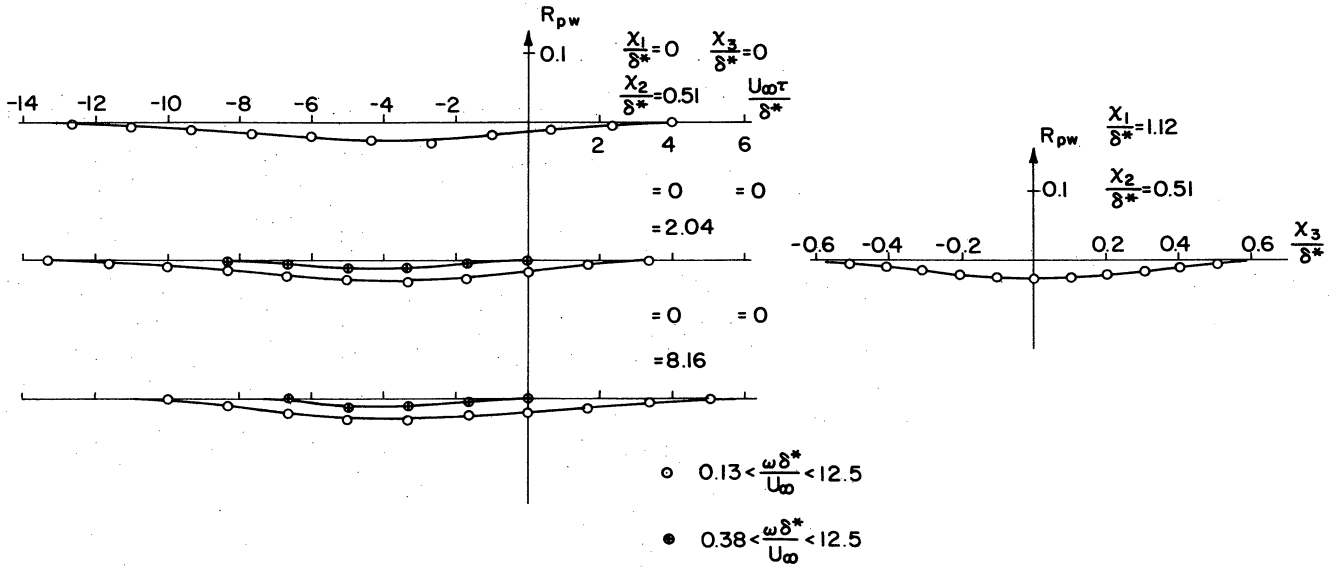

Fig. 28. Measured values of the space-time correlation of fluctuating transverse velocity with fluctuating wall pressure showing the effect of extraneous large-scale flow disturbance caused by Taylor-Goertler vortices and density stratification.

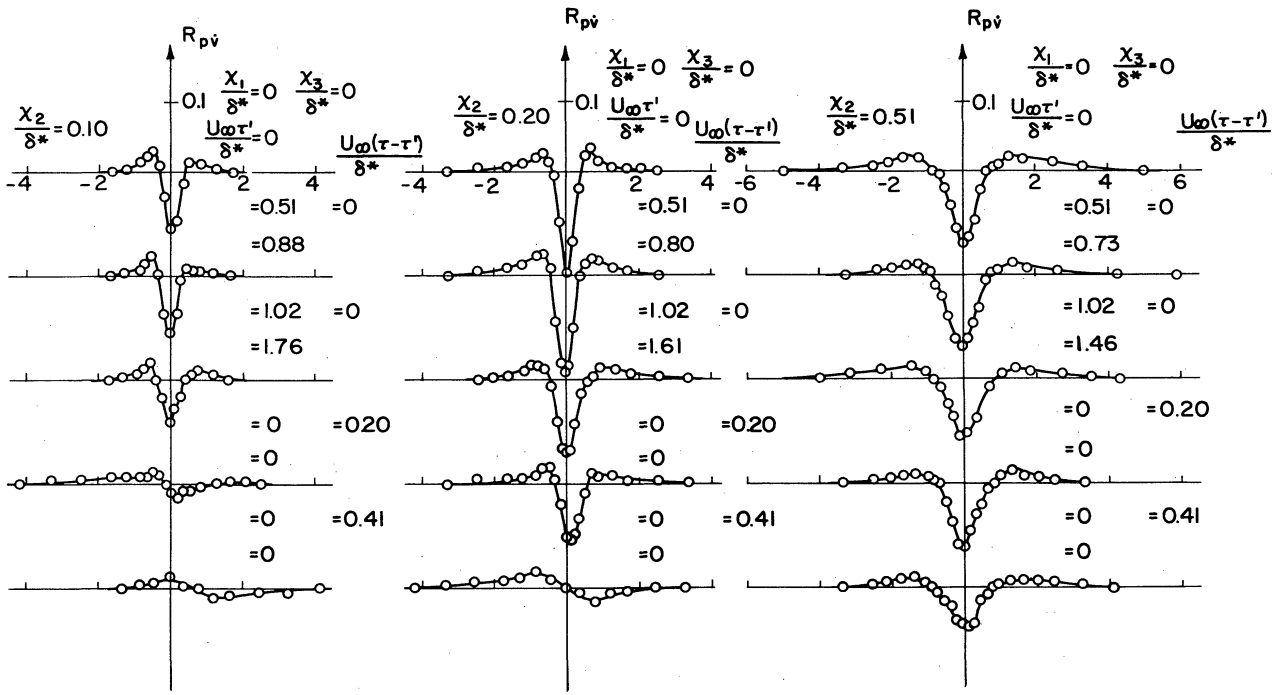

Fig. 29. Measured values of the space-time correlation of the time derivative of fluctuating velocity normal to the wall with fluctuating wall pressure.

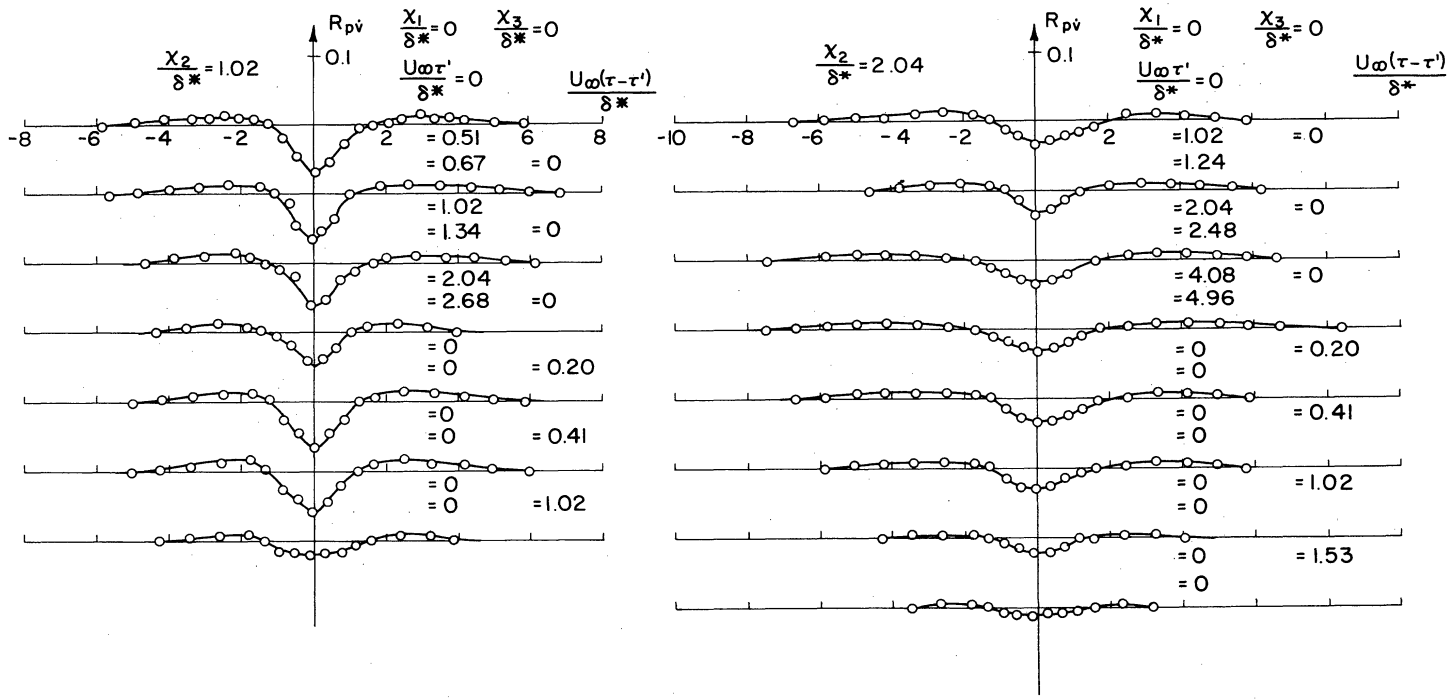

Fig. 30. Measured values of the space-time correlation of the time derivative of fluctuating velocity normal to the wall with fluctuating wall pressure.

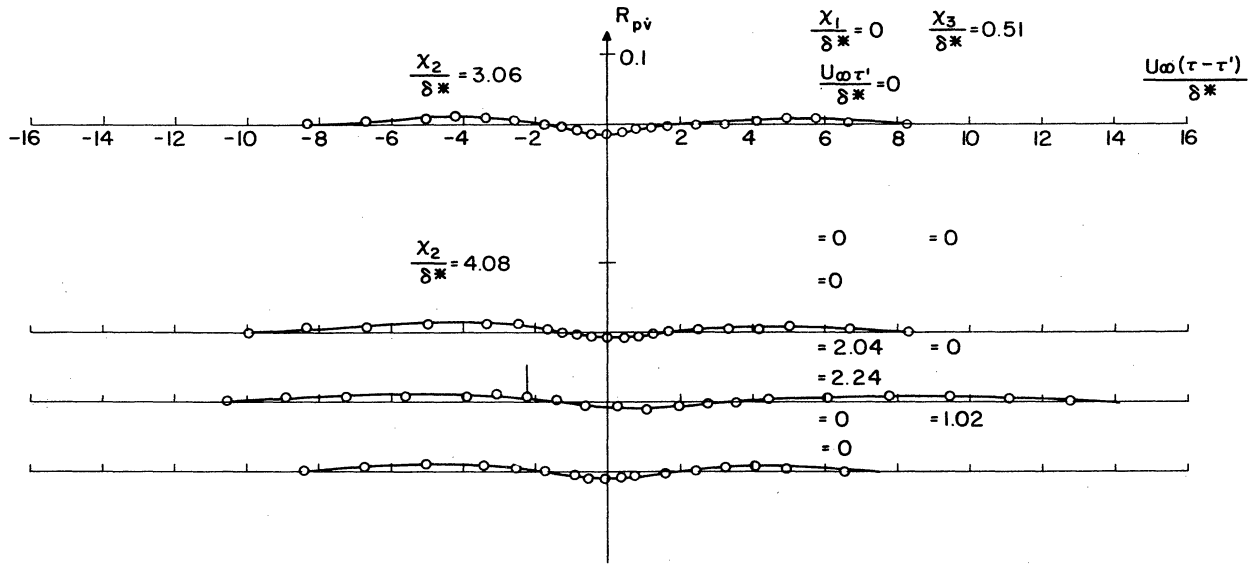

Fig. 31. Measured values of the space-time correlation of the time derivative of fluctuating velocity normal to the wall with fluctuating wall pressure.

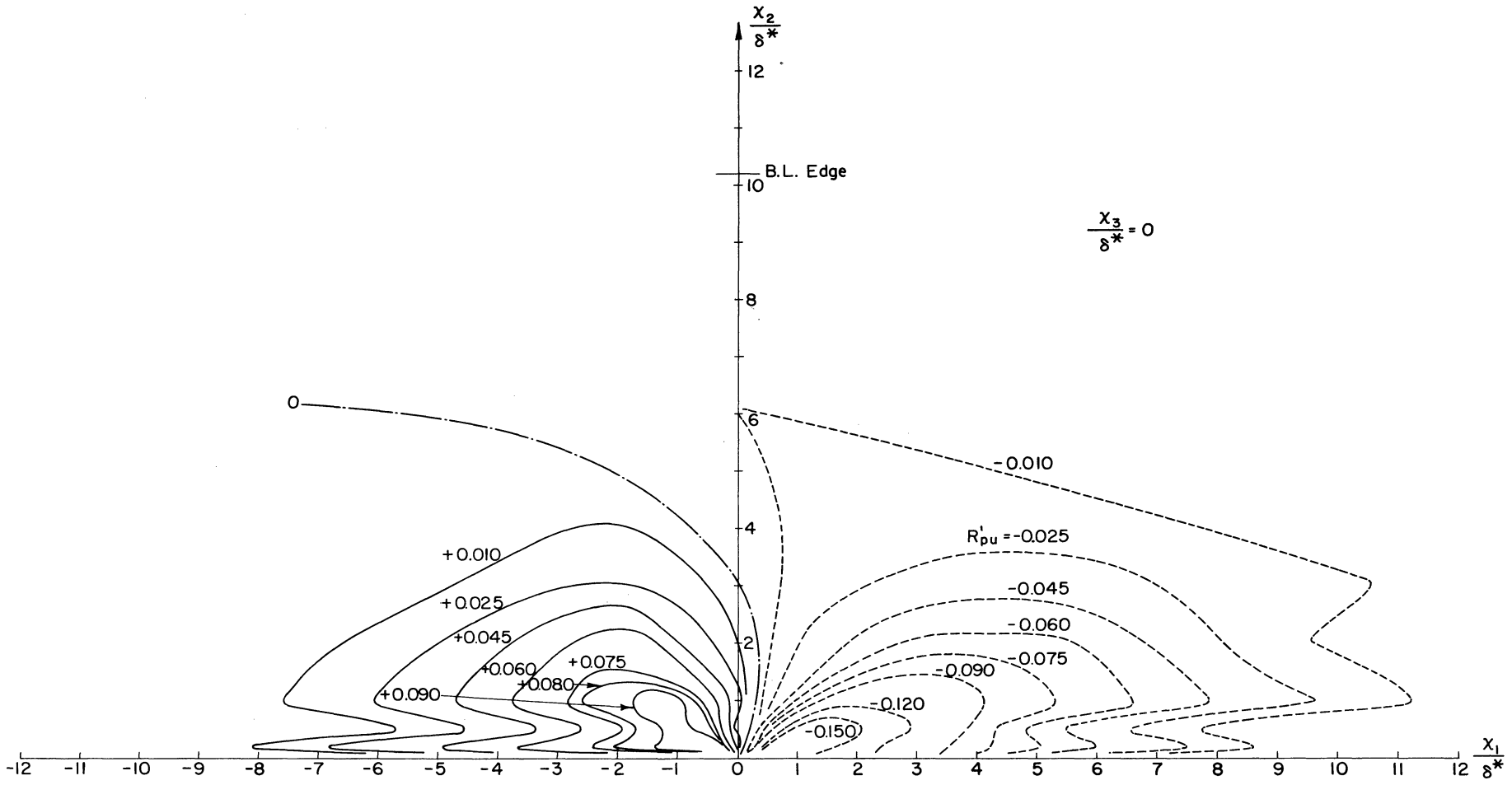

Fig. 32. Correlation contours of R'_{pu} in the x_1-x_2 plane. Correlation normalized on the value of the velocity fluctuation at $x_2/\delta^* = 0.51$. Origin of coordinate system at pressure transducer.

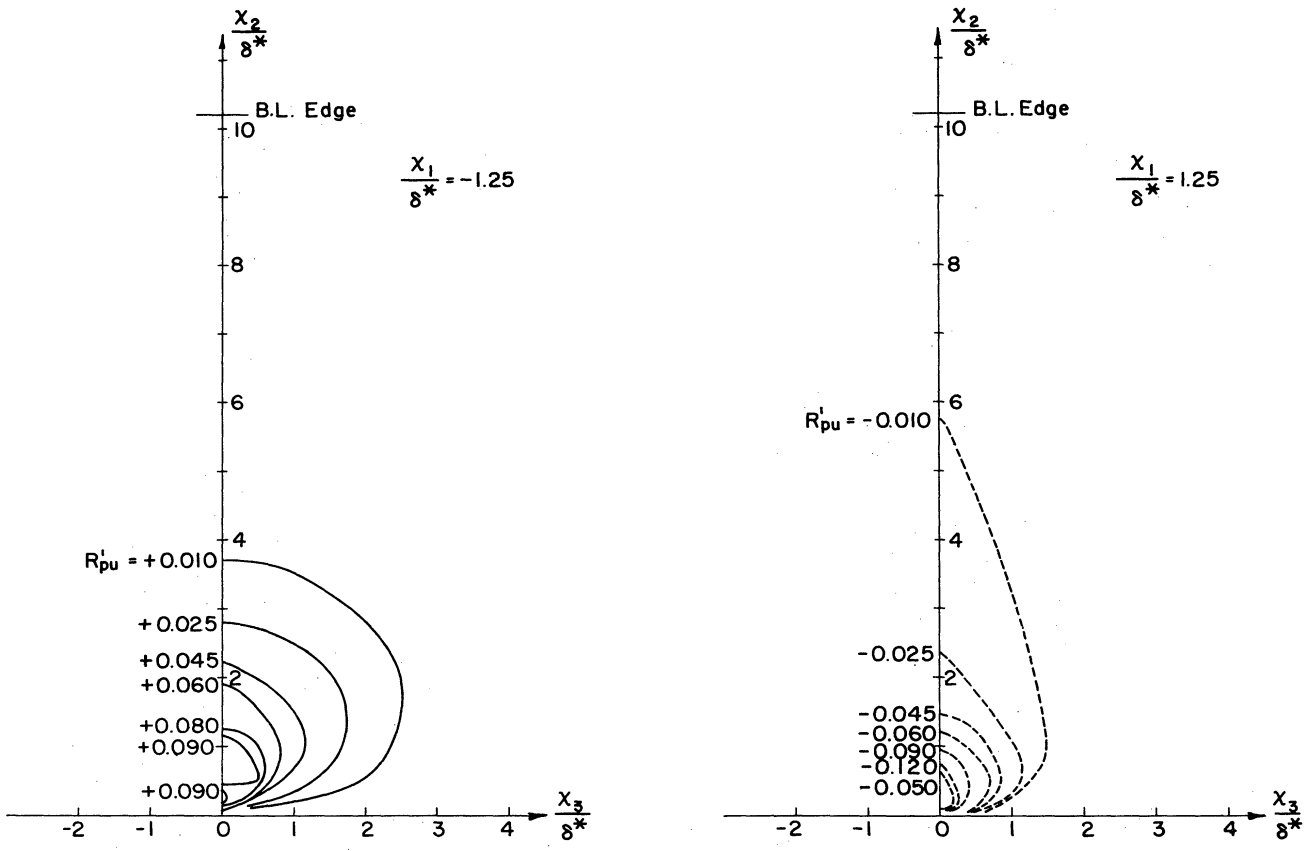

Fig. 33. Correlation contours of R'_{pu} in the x_2-x_3 plane. Correlation normalized on the value of the velocity fluctuation at $x_2/\delta^* = 0.51$. Origin of coordinate system at pressure transducer.

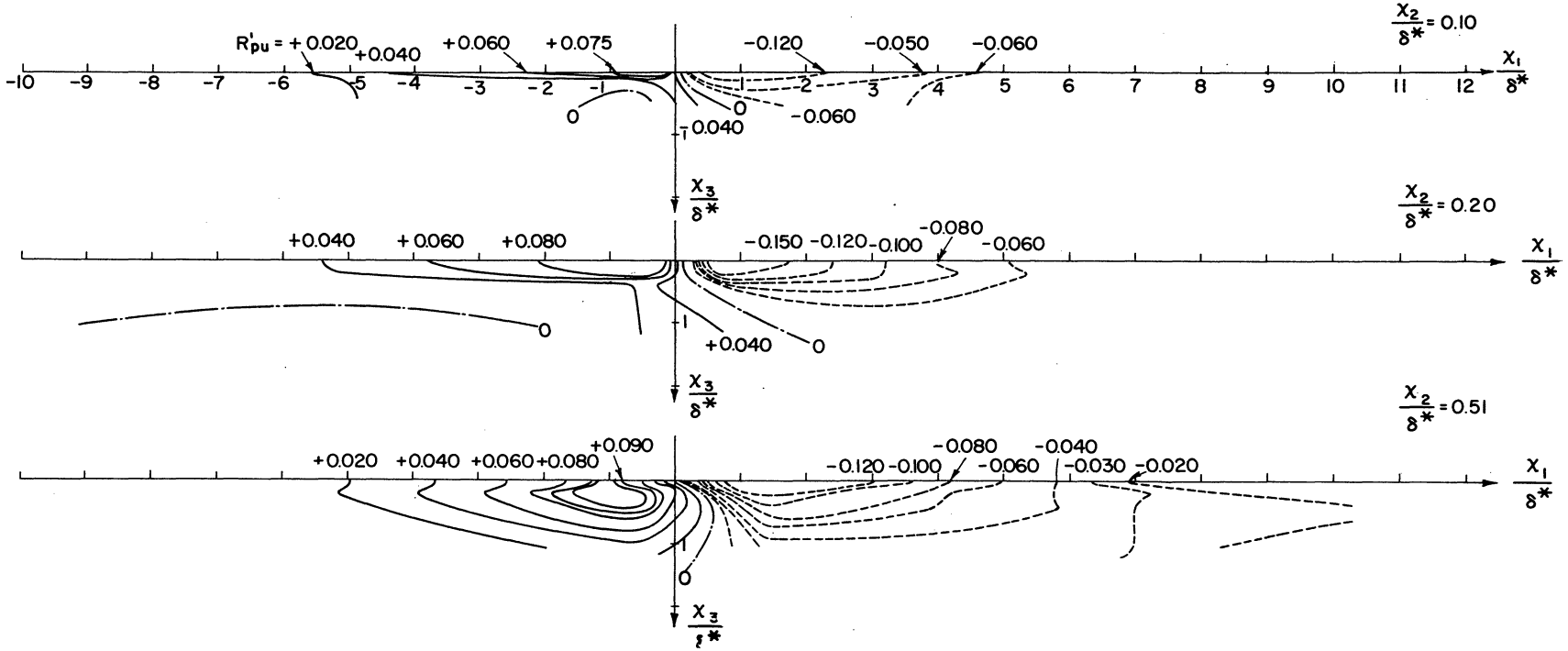

Fig. 34. Correlation contours of R'_{pu} in the x_1-x_3 plane. Correlation normalized on the value of the velocity fluctuation at $x_2/\delta^* = 0.51$. Origin of coordinate system at pressure transducer.

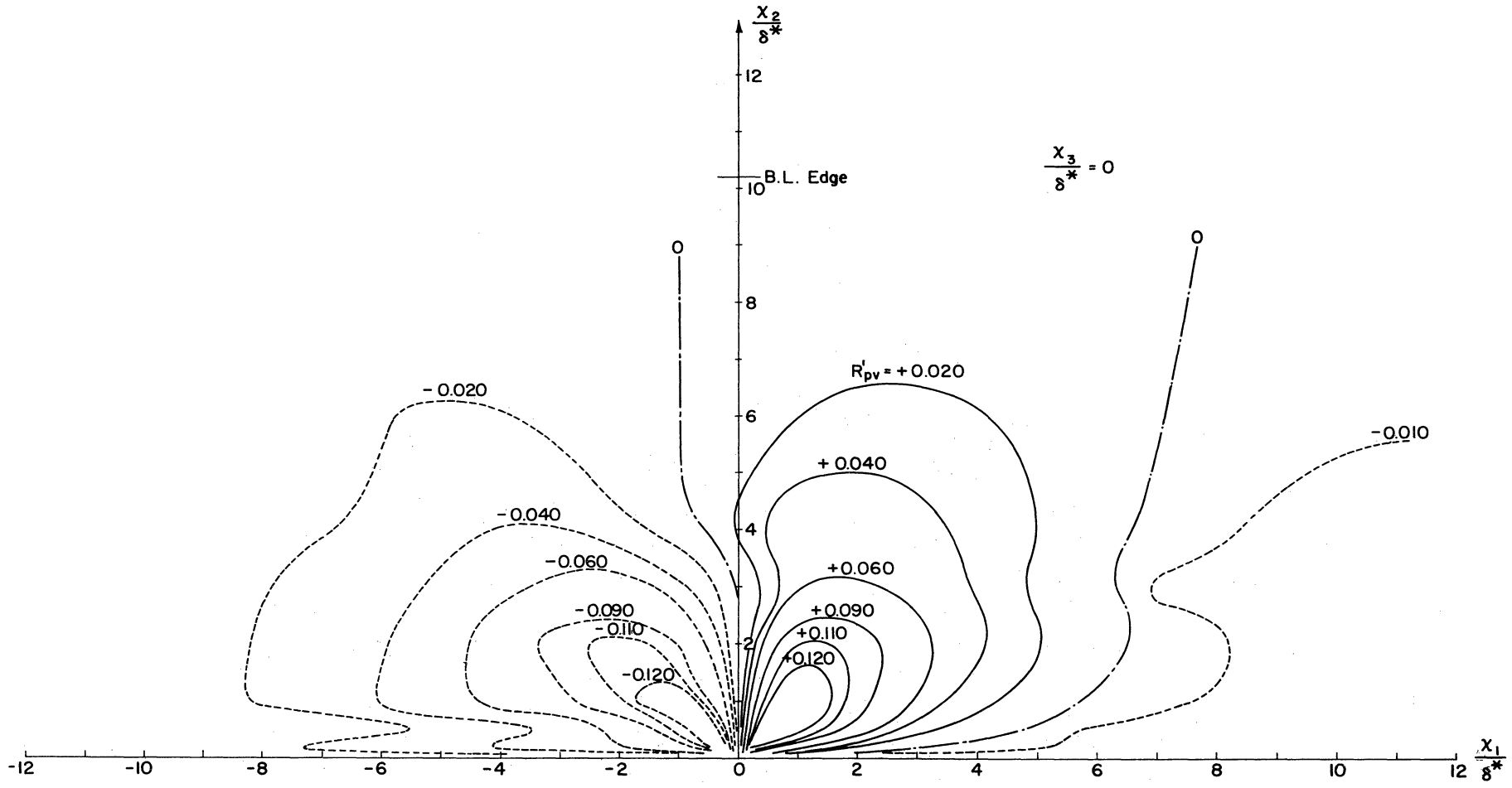

Fig. 35. Correlation contours of R'_{pv} in the x_1-x_2 plane. Correlation normalized on the value of the velocity fluctuation at $x_2/\delta^* = 0.51$. Origin of coordinate system at pressure transducer.

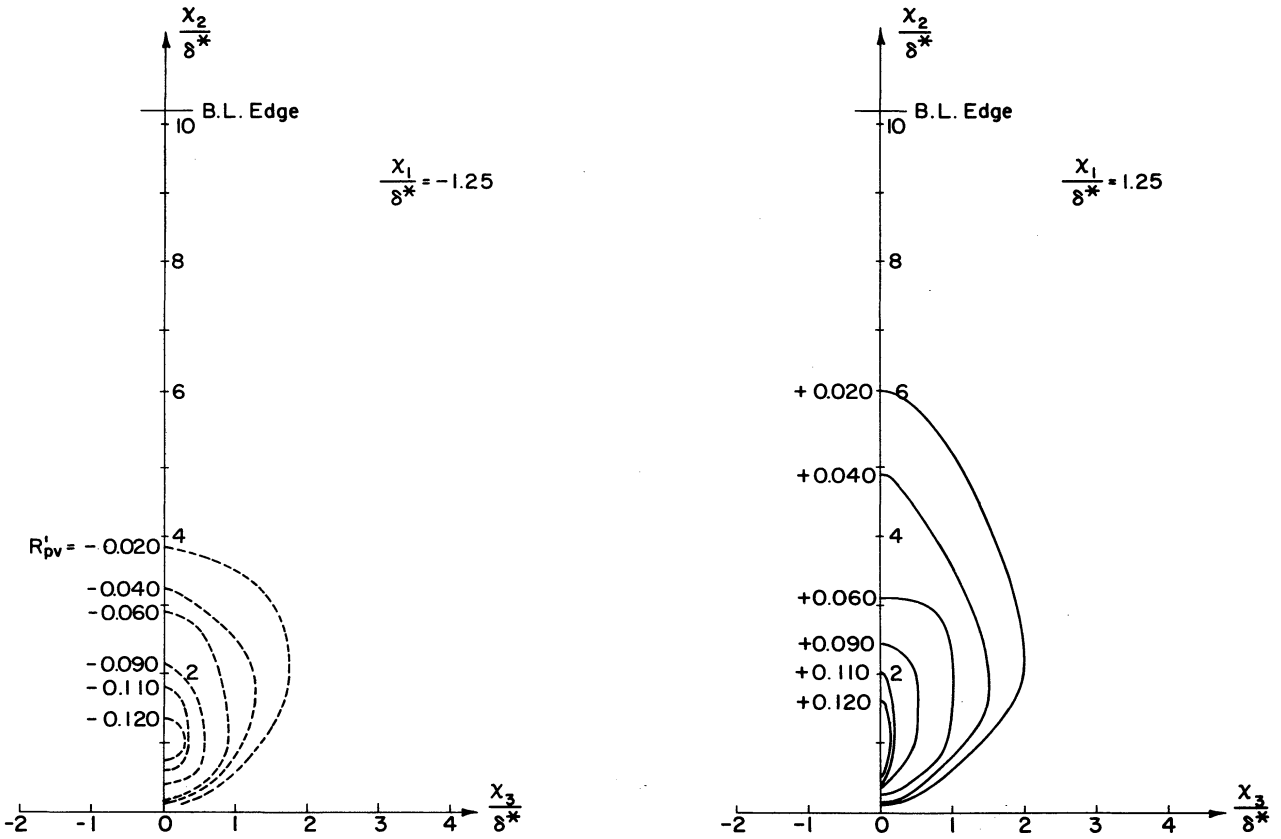

Fig. 36. Correlation contours of R'_{pv} in the x_2-x_3 plane. Correlation normalized on the value of the velocity fluctuation at $x_2/\delta^* = 0.51$. Origin of coordinate system at pressure transducer.

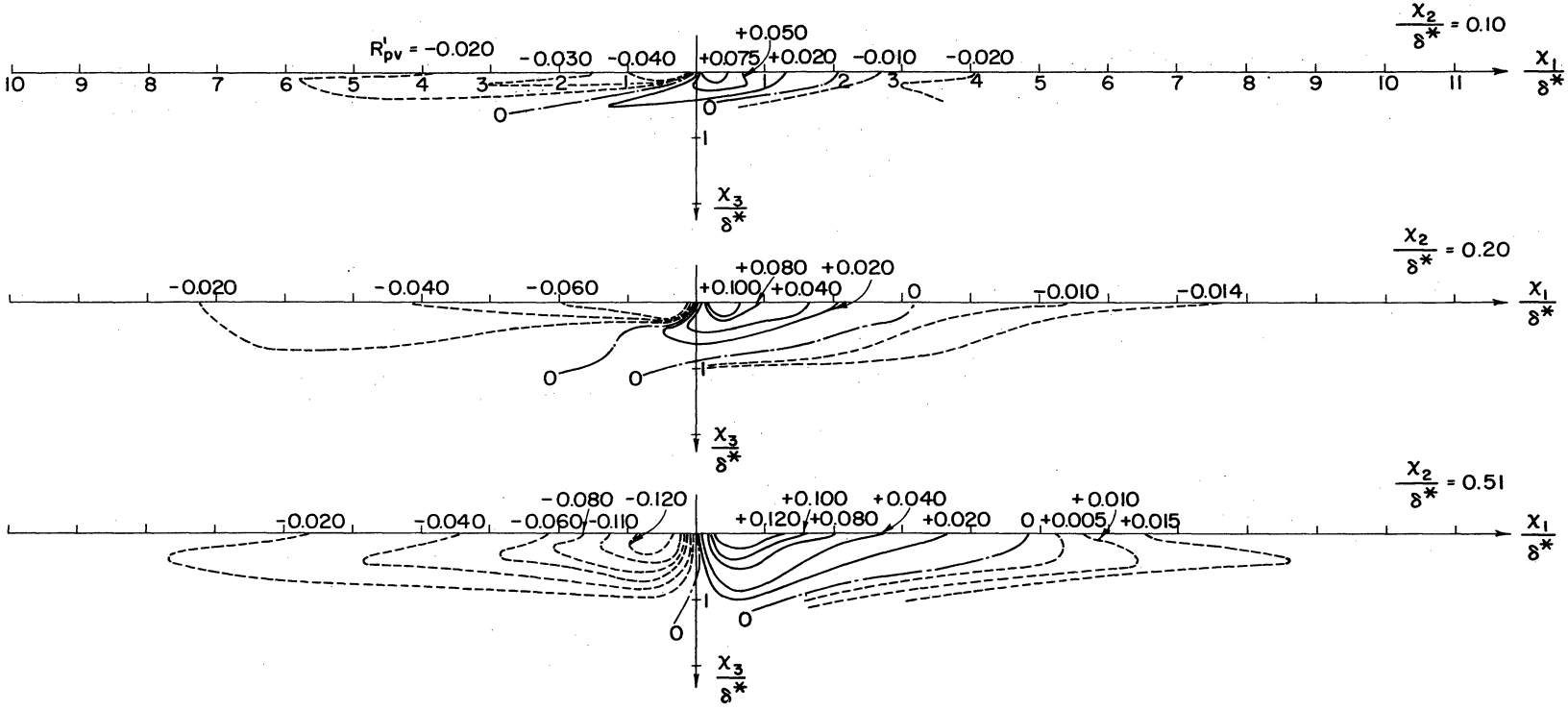

Fig. 37. Correlation contours of R'_{pv} in the x_1-x_3 plane. Correlation normalized on the value of the velocity fluctuation at $x_2/\delta^* = 0.51$. Origin of coordinate system at pressure transducer.

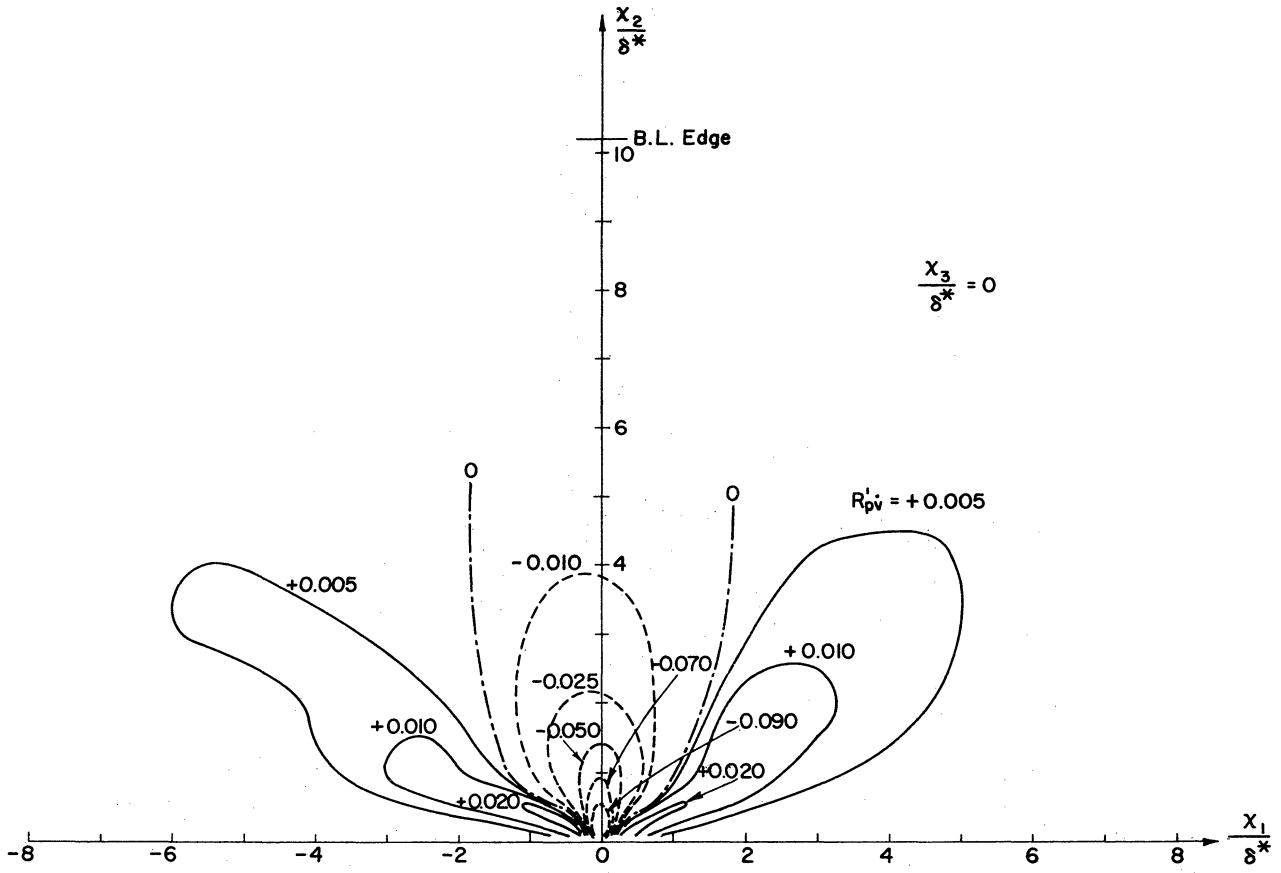

Fig. 38. Correlation contours of $R'_{p\dot{v}}$ in the x_1-x_2 plane. Correlation normalized on the value of the velocity fluctuation derivative at $x_2/\delta^* = 0.51$. Origin of coordinate system at pressure transducer.

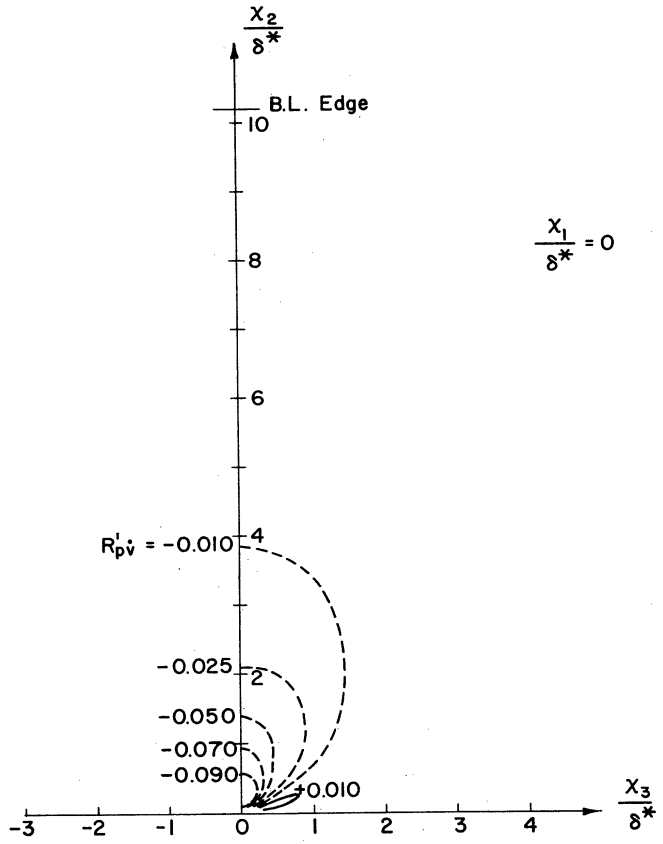

Fig. 39. Correlation contours of R'_{pv} in the x_2-x_3 plane. Correlation normalized on the value of the velocity fluctuation derivative at $x_2/\delta^* = 0.51$. Origin of coordinate system at pressure transducer.

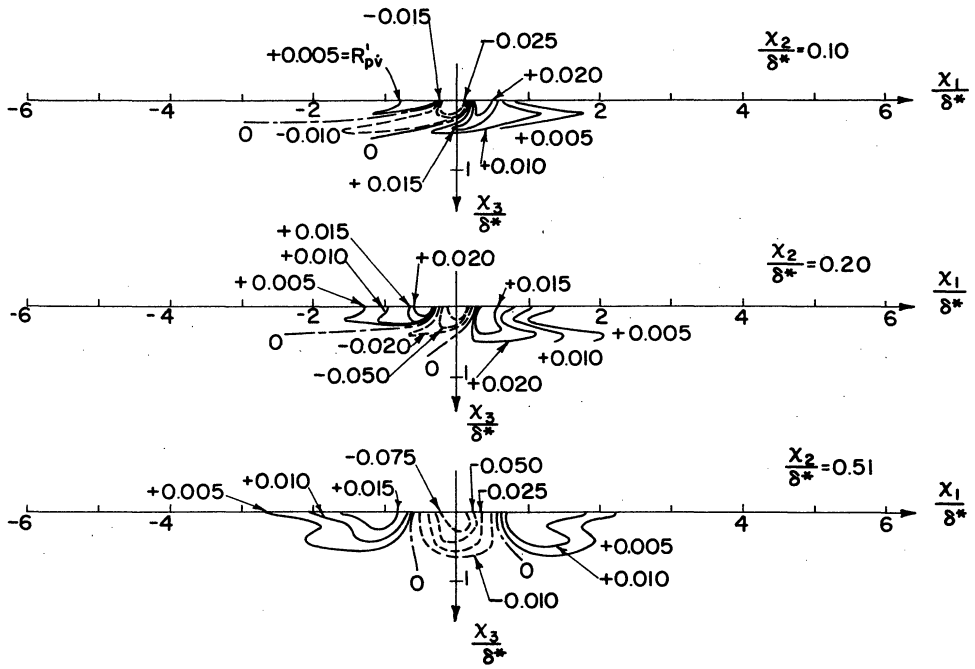

Fig. 40. Correlation contours of R'_{pv} in the x_1-x_3 plane. Correlation normalized on the value of the velocity fluctuation derivative at $x_2/\delta^* = 0.51$. Origin of coordinate system at pressure transducer.

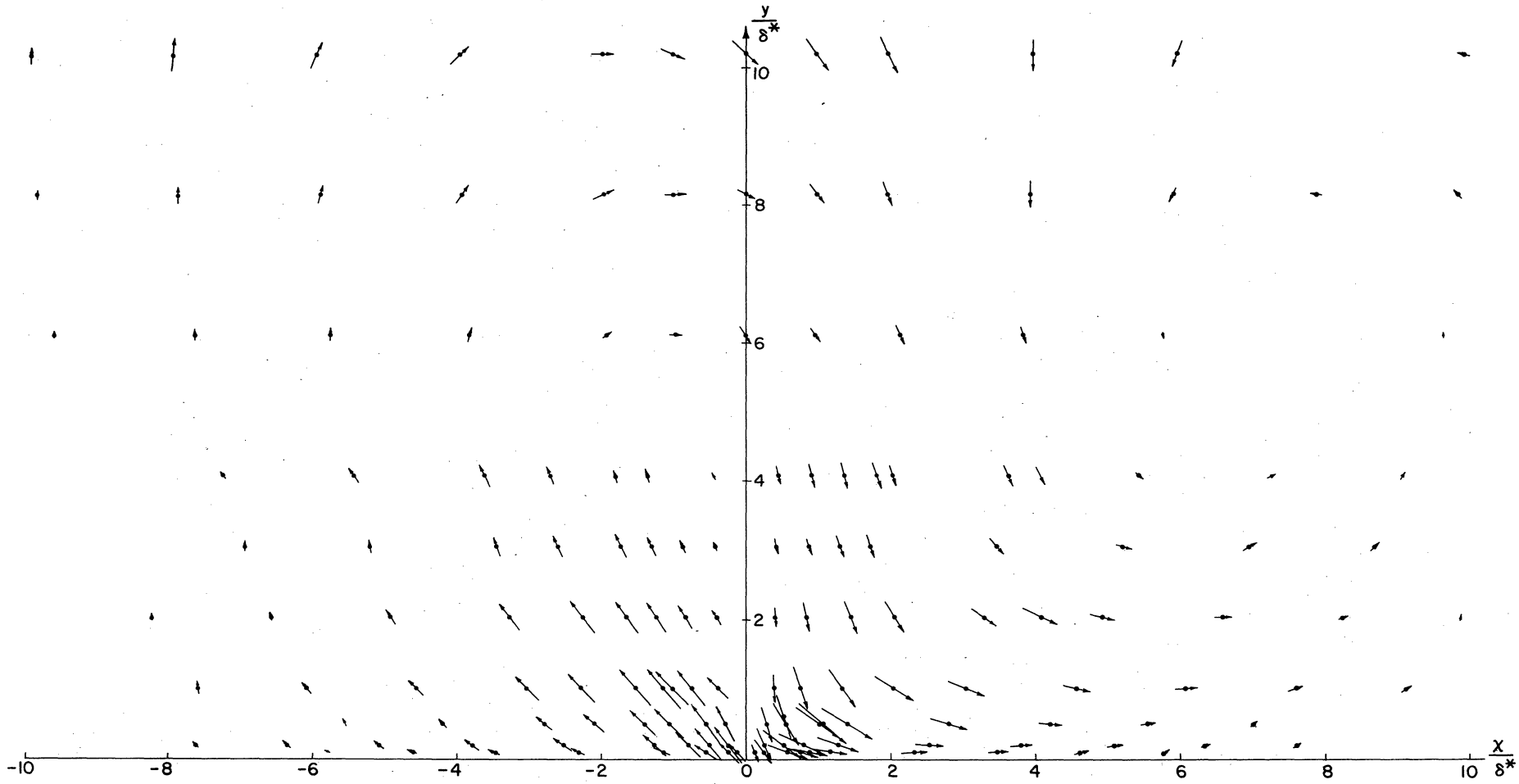

Fig. 41. Vector Field of Correlation. Magnitude of the vector at any point is $\sqrt{R_{pu}^2 + R_{pv}^2}$. Direction of the vector at any point as measured from the positive x_1-axis is given by $\tan^{-1} \frac{R_{pv}}{R_{pu}}$.

DISTRIBUTION LIST
(One copy unless otherwise noted)

Chief of Naval Research
Department of the Navy
Washington 25, D. C.
Attn: Code 438 3
Attn: Code 461
Attn: Code 463
Attn: Code 466

Commanding Officer
Office of Naval Research
Branch Office
495 Summer Street
Boston 10, Massachusetts

Commanding Officer
Office of Naval Research
Branch Office
346 Broadway
New York 13, New York

Commanding Officer
Office of Naval Research
Branch Office
1030 East Green Street
Pasadena, California

Commanding Officer
Office of Naval Research
Branch Office
1000 Geary Street
San Francisco 9, California

Commanding Officer 10
Office of Naval Research
Branch Office
Navy No. 100, Fleet Post Office
New York, New York

Director 6
Naval Research Laboratory
Washington 25, D. C.
Attn: Code 2027

Chief, Bureau of Naval Weapons
Department of the Navy
Washington 25, D. C.
Attn: Code RUAW-4
Attn: Code RRRE
Attn: Code RAAD
Attn: Code RAAD-222
Attn: Code DIS-42

Chief, Bureau of Ships
Department of the Navy
Washington 25, D. C.
Attn: Code 310
Attn: Code 312
Attn: Code 335
Attn: Code 420
Attn: Code 421
Attn: Code 440
Attn: Code 442
Attn: Code 449

Chief, Bureau of Yards and Docks
Department of the Navy
Washington 25, D. C.
Attn: Code D-400

Commanding Officer and Director
David Taylor Model Basin
Washington 7, D. C.
Attn: Code 108
Attn: Code 142
Attn: Code 500
Attn: Code 513
Attn: Code 520
Attn: Code 526
Attn: Code 526A
Attn: Code 530
Attn: Code 533
Attn: Code 580
Attn: Code 585
Attn: Code 589
Attn: Code 591
Attn: Code 591A
Attn: Code 700

DISTRIBUTION LIST (Continued)

Commander
U. S. Naval Ordnance Test Station
China Lake, California
Attn: Code 753

Commander
U. S. Naval Ordnance Test Station
Pasadena Annex
3202 E. Foothill Blvd.
Pasadena 8, California
Attn: Code P-508

Commander
Planning Department
Portsmouth Naval Shipyard
Portsmouth, New Hampshire

Commander
Planning Department
Boston Naval Shipyard
Boston 29, Massachusetts

Commander
Planning Department
Pearl Harbor Naval Shipyard
Navy No. 128, Fleet Post Office
San Francisco, California

Commander
Planning Department
San Francisco Naval Shipyard
San Francisco 24, California

Commander
Planning Department
Mare Island Naval Shipyard
Vallejo, California

Commander
Planning Department
New York Naval Shipyard
Brooklyn 1, New York

Commander
Planning Department
Puget Sound Naval Shipyard
Bremerton, Washington

Commander
Planning Department
Philadelphia Naval Shipyard
U. S. Naval Base
Philadelphia 12, Pennsylvania

Commander
Planning Department
Norfolk Naval Shipyard
Portsmouth, Virginia

Commander
Planning Department
Charleston Naval Shipyard
U. S. Naval Base
Charleston, South Carolina

Commander
Planning Department
Long Beach Naval Shipyard
Long Beach 2, California

Commander
Planning Department
U. S. Naval Weapons Laboratory
Dahlgren, Virginia

Commander
U. S. Naval Ordnance Laboratory
White Oak, Maryland

Dr. A. V. Hershey
Computation and Exterior
Ballistics Laboratory
U. S. Naval Weapons Laboratory
Dahlgren, Virginia

Superintendent
U. S. Naval Academy
Annapolis, Maryland
Attn: Library

DISTRIBUTION LIST (Continued)

Superintendent
U. S. Naval Postgraduate School
Monterey, California

Commandant
U. S. Coast Guard
1300 E Street, N. W.
Washington, D. C.

Secretary Ship Structure Committee
U. S. Coast Guard Headquarters
1300 E Street, N. W.
Washington, D. C.

Commander
Military Sea Transportation Service
Department of the Navy
Washington 25, D. C.

U. S. Maritime Administration
GAO Building
441 G Street, N. W.
Washington, D. C.
Attn: Division of ship Design
Attn: Division of Research

Superintendent
U. S. Merchant Marine Academy
Kings Point, Long Island, New York
Attn: Capt. L. S. McCready (Dept. of Engineering)

Commanding Officer and Director
U. S. Navy Mine Defense Laboratory
Panama City, Florida

Commanding Officer
NROTC and Naval Administrative Unit
Massachusetts Institute of Technology
Cambridge 39, Massachusetts

U. S. Army Transportation Research and Development Command 2
Fort Eustis, Virginia
Attn: Marine Transport Division

Director of Research
National Aeronautics and Space Administration
1512 H Street, N. W.
Washington 25, D. C.

Director
Langley Research Center
Langley Field Virginia
Attn: Mr. J. B. Parkinson 2
Attn: Mr. I. E. Garrick
Attn: Mr. D. J. Marten

Director Engineering Sciences Division
National Science Foundation
1951 Constitution Avenue, N. W.
Washington 25, D. C.

Director
National Bureau of Standards
Washington 25, D. C.
Attn: Fluid Mechanics Division (Dr. G. B. Schubauer)
Attn: Dr. G. H. Keulegan
Attn: Dr. J. M. Franklin

Armed Services Technical Information Agency 10
Arlington Hall Station
Arlington 12, Virginia

Office of Technical Services
Department of Commerce
Washington 25, D. C.

California Institute of Technology
Pasadena 4, California
Attn: Professor M. S. Plesset
Attn: Professor T. Y. Wu
Attn: Professor A. J. Acosta

University of California
Department of Engineering
Los Angeles 24, California
Attn: Dr. A. Powell

DISTRIBUTION LIST (Continued)

Director
Scripps Institute of Oceanography
University of California
La Jolla, California

Professor M. L. Albertson
Department of Civil Engineering
Colorado A and M College
Fort Collins, Colorado

Professor J. E. Cermak
Department of Civil Engineering
Colorado State University
Fort Collins, Colorado

Professor W. R. Sears
Graduate School of Aeronautical Engr.
Cornell University
Ithaca, New York

State University of Iowa
Iowa Inst. of Hydraulic Research
Iowa City, Iowa
Attn: Dr. H. Rouse
Attn: Dr. L. Landweber

Harvard University
Cambridge 38, Massachusetts
Attn: Professor G. Birkhoff
(Dept. of Mathematics)
Attn: Professor G. F. Carrier
(Dept. of Mathematics)

Massachusetts Institute of Technology
Cambridge 39, Massachusetts
Attn: Department of Naval Architecture and Marine Engineering
Attn: Professor A. T. Ippen

University of Michigan
Ann Arbor, Michigan
Attn: Professor R. B. Couch
(Dept. of Naval Architecture)
Attn: Professor W. W. Willmarth
(Aero. Engrg. Department)
Attn: Professor M. S. Uberoi
(Aero. Engrg. Department)

Dr. L. G. Straub, Director
St. Anthony Falls Hydraulic Lab
University of Minnesota
Minneapolis 14, Minnesota
Attn: Mr. J. N. Wetzel
Attn: Professor B. Silberman

Professor J. J. Foody
Engineering Department
New York State University Maritime College
Fort Schuyler, New York

New York University
Institute of Mathematical Sciences
25 Waverly Place
New York 3, New York
Attn: Professor J. Keller
Attn: Professor J. J. Stoker
Attn: Professor R. Kraichnan

The Johns Hopkins University
Department of Mechanical Engineering
Baltimore 18, Maryland
Attn: Professor S. Corrsin
Attn: Professor O. M. Phillips 2

Massachusetts Institute of Technology
Department of Naval Architecture and Marine Engineering
Cambridge 39, Massachusetts
Attn: Prof. M. A. Abkowitz, Head

Dr. G. F. Wislicenus
Ordnance Research Laboratory
Pennsylvania State University
University Park, Pennsylvania
Attn: Dr. M. Sevik

Professor R. C. DiPrima
Department of Mathematics
Rensselaer Polytechnic Institute
Troy, New York

DISTRIBUTION LIST (Continued)

Stevens Institute of Technology
Davidson Laboratory
Castle Point Station
Hoboken, New Jersey
Attn: Professor E. V. Lewis
Attn: Mr. D. Savitsky
Attn: Mr. J. P. Breslin
Attn: Mr. C. J. Henry
Attn: Mr. S. Tsakonas

Webb Institute of Naval Architecture
Crescent Beach Road
Glen Cove, New York
Attn: Technical Library

Director
Woods Hole Oceanographic Institute
Woods Hole, Massachusetts

Commander
Air Research and Development Command
Air Force Office of Scientific Research
14th and Constitution
Washington 25, D. C.
Attn: Mechanics Branch

Commander
Wright Air Development Division
Aircraft Laboratory
Wright-Patterson Air Force Base, Ohio
Attn: Mr. W. Mykytow, Dynamics Branch

Cornell Aeronautical Laboratory
4455 Genesee Street
Buffalo, New York
Attn: Mr. W. Targoff
Attn: Mr. R. White

Massachusetts Institute of Technology
Fluid Dynamics Research Laboratory
Cambridge 39, Massachusetts
Attn: Professor H. Ashley
Attn: Professor M. Landahl
Attn: Professor J. Dugundji

Hamburgische Schiffbau-Versuchsanstalt
Bramfelder Strasse 164
Hamburg 33, Germany
Attn: Dr. O. Grim
Attn: Dr. H. W. Lerbs

Institut für Schiffbau der
Universität Hamburg
Berliner Tor 21
Hamburg 1, Germany
Attn: Professor G. P. Weinblum, Director

Max-Planck Institut für Strömungsforschung
Bottingerstrasse 6/8
Gottingen, Germany
Attn: Dr. H. Reichardt

Hydro-og Aerodynamisk Laboratorium
Lyngby, Denmark
Attn: Professor Carl Prohaska

Skipsmodelltanken
Trondheim, Norway
Attn: Professor J. K. Lunde

Versuchsanstalt für Wasserbau und Schiffbau
Schleuseninsel im Tiergarten
Berlin, Germany
Attn: Dr. S. Schuster, Director

Technische Hogeschool
Institut voor Toegepaste Wiskunde
Julianalaan 132
Delft, Netherlands
Attn: Professor R. Timman

DISTRIBUTION LIST (Continued)

Bureau D'Analyse et de Techerche
Appliquees
47 Avenue Victor Cresson
Issy les Moulineaux (Seine)
Paris, France
Attn: Professor Siestrunck

Netherlands Ship Model Basin
Wageningen, Netherlands
Attn: Dr. Ir. J. D. van Manen

National Physical Laboratory
Teddington, Middlesex, England
Attn: Dr. F. H. Todd, Superintendent
Ship Division
Attn: Head Aerodynamics Division
Attn: Mr. A. Silverleaf

Head, Aerodynamics Department 2
Royal Aircraft Establishment
Farnborough, Hants, England
Attn: Mr. M. O. W. Wolfe

Boeing Airplane Co.
Seattle Division
Seattle, Washington
Attn: Mr. M. J. Turner

Electric Boat Division
General Dynamics Corporation
Groton, Connecticut
Attn: Mr. Robert McCandliss

General Applied Sciences Labs, Inc.
Merrick and Stewart Avenues
Westbury, Long Island, New York

Gibbs and Cox, Inc.
21 West Street
New York, New York

Grumman Aircraft Engineering Corp.
Bethpage, Long Island, New York
Attn: Mr. E. Baird
Attn: Mr. E. Bower

Grumman Aircraft Engineering Corp.
Dynamic Developments Division
Babylon, New York

Lockheed Aircraft Corporation
Missiles and Space Division
Palo Alto, California
Attn: R. W. Kermeen

Midwest Research Institute
425 Volker Blvd.
Kansas City 10, Missouri
Attn: Mr. Zeydel

Director, Department of Mechanical
Sciences
Southwest Research Institute
8500 Culebra Road
San Antonio 6, Texas
Attn: Dr. H. N. Abramson
Attn: Mr. G. Ransleben
Attn: Editor, Applied Mechanics
Review

Convair
A Division of General Dynamics
San Diego, California
Attn: Mr. R. H. Oversmith
Attn: Mr. A. D. MacLellan
Attn: Mr. H. T. Brooke

Dynamic Developments, Inc.
15 Berry Hill Road
Oyster Bay, Long Island, New York

Dr. S. F. Hoerner
148 Busteed Drive
Midland Park, New Jersey

Hydronautics, Incorporated
200 Monroe Street
Rockville, Maryland
Attn: Mr. Phillip Eisenberg

Rand Development Corporation
13600 Deise Avenue
Cleveland 10, Ohio
Attn: Dr. A. S. Iberall

U. S. Rubber Company
Research and Development Department
Wayne, New Jersey
Attn: Mr. L. M. White

Technical Research Group, Inc.
2 Aerial Way
Syosset, Long Island, New York
Attn: Mr. Jack Kotik
Attn: Dr. Sheldon Gardner